American Society of Naturalists

Spatial Waves of Advance with Bistable Dynamics: Cytoplasmic and Genetic Analogues of Allee Effects

N. H. Barton[1] and Michael Turelli[2],*

1. Institute of Science and Technology Austria, Am Campus 1, A-3400 Klosterneuburg, Austria;   2. Department of Evolution and Ecology, University of California, Davis, California 95616

abstract: Unlike unconditionally advantageous "Fisherian" variants that tend to spread throughout a species range once introduced anywhere, "bistable" variants, such as chromosome translocations, have two alternative stable frequencies, absence and (near) fixation. Analogous to populations with Allee effects, bistable variants tend to increase locally only once they become sufficiently common, and their spread depends on their rate of increase averaged over all frequencies. Several proposed manipulations of insect populations, such as using *Wolbachia* or "engineered underdominance" to suppress vector-borne diseases, produce bistable rather than Fisherian dynamics. We synthesize and extend theoretical analyses concerning three features of their spatial behavior: rate of spread, conditions to initiate spread from a localized introduction, and wave stopping caused by variation in population densities or dispersal rates. Unlike Fisherian variants, bistable variants tend to spread spatially only for particular parameter combinations and initial conditions. Wave initiation requires introduction over an extended region, while subsequent spatial spread is slower than for Fisherian waves and can easily be halted by local spatial inhomogeneities. We present several new results, including robust sufficient conditions to initiate (and stop) spread, using a one-parameter cubic approximation applicable to several models. The results have both basic and applied implications.

Keywords: Wolbachia, underdominance, population replacement, species invasions, critical propagule size, wave stopping.

* Corresponding author; e-mail: mturelli@ucdavis.edu.

Introduction

There is increasing interest in manipulating arthropod disease-vector and pest populations by introducing maternally inherited bacteria or genetic elements whose frequency tends to decline when they are rare but increase once they become sufficiently common (e.g., Brownstein et al. 2003; Rasgon et al. 2003; Magori and Gould 2006; Sinkins and Gould 2006; Moreira et al. 2009). These dynamics are analogous to those of underdominant chromosome arrangements (i.e., heterokaryotypes less fit than both homokaryotyes) that occur in natural hybrid zones (White 1973, chap. 11). Underdominant karyotypes motivated early suggestions for genetic manipulation of disease-vector populations (e.g., Curtis 1968; Whitten 1971). The spatial dynamics of such variants were first described in the evolutionary genetics literature by Bazykin (1969) and Barton (1979a) and in the mathematics literature by Aronson and Weinberger (1975). These dynamics are similar to the population dynamics of invasive species with (strong) Allee effects, namely, species that decline at low densities, so that populations tend to increase only above a critical density threshold (Wang and Kot 2001; Taylor and Hastings 2005). These genetic and ecological systems are "bistable," possessing two locally stable equilibria: one at zero frequency or density and another at high frequency or density. Spatial locations where transitions occur between alternative genetic equilibria have been called "tension zones" (Key 1968; Barton and Hewitt 1989).

Bistable systems are common in applied mathematics, arising, for instance, in neurobiology (Hodgkin and Huxley 1952; Nagumo et al. 1962, 1965; reviewed in Keener and Sneyd 2004, chap. 9), the chemistry of combustion (Zeldovich and Barenblatt 1959), and quantum physics (Coleman 1977). Spatial models with bistable dynamics have attracted a great deal of attention from mathematicians (e.g., Aronson and Weinberger 1975; Fife and McLeod 1977; Bramson 1983), who have generally focused on the asymptotic behavior of traveling waves, emphasizing conditions that lead to spread and approximations for ultimate wave speed. Most analyses of invasions and introductions in population biology also focus on the rate at which invading species or novel variants spread spatially (Shigesada and Kawasaki 1997; Taylor and Hastings 2005; Tobin et al. 2007). We will focus on two other aspects of bistable spatial dynamics.

The existence of an unstable point means that in an isolated population, there is a critical frequency that must be exceeded for local deterministic increase to occur.

(Throughout, we use "frequency" to refer to the variable of interest: allele frequency, proportion infected, or population density, relative to carrying capacity.) In spatially distributed populations, this produces two related effects. The first we refer to as the "critical propagule size." If a spatially concentrated introduction is assumed, how many individuals must be introduced to initiate an expanding wave? Obviously, the critical frequency must be exceeded locally, but over how large an area must this be done—and by how much must the threshold be exceeded—for the variant to spread rather than being swamped by immigration? The second effect is that unlike "Fisherian waves" of genetic variants (Fisher 1937) or species (Skellam 1951) that tend to spread throughout the range, irrespective of heterogeneities in habitat quality or barriers to dispersal, waves of advance for bistable variants can easily be stopped by local decreases in migration rates and/or increases in population densities (Barton 1979*a*). This has been rediscovered as "range pinning" for species invasions (Keitt et al. 2001).

The diffusive spread of an unconditionally favored allele or species was first analyzed by Fisher (1937), Kolmogorov et al. (1937), and Skellam (1951). Bazykin (1969) initiated spatial analyses of bistable genetic models, providing an explicit solution for the shape of a one-dimensional hybrid zone under weak symmetric underdominance (i.e., the special case in which both homozygotes are equally superior to heterozygotes). With asymmetric underdominance, he asserted that the fitter homozygote would tend to spread spatially but that its spread would be halted by barriers to dispersal. Barton (1979*a*) generalized and extended Bazykin's (1969) analysis, providing explicit descriptions of the traveling waves, conditions for wave stopping, and approximations for the critical propagule size needed to initiate a traveling wave. Barton and Hewitt (1989) reviewed this work and described in more detail how tension zones move across heterogeneous landscapes.

Ecologists have focused on the consequences of Allee effects for species invasions (Lewis and Kareiva 1993; Taylor and Hastings 2005) and have considered both initial conditions for establishing successful invasions (Lewis and Kareiva 1993; Soboleva et al. 2003) and conditions for stopping them ("range pinning"; Keitt et al. 2001). In contrast to the many useful syntheses of data and theory concerning wave speeds, there have been relatively few attempts to relate data or proposed experiments to the theoretical results concerning critical propagule sizes and wave stopping (but see Nichols and Hewitt 1986).

We will review, synthesize, and extend the mathematical results concerning wave speed, the initial propagule size needed to start a traveling wave, and the nature of inhomogeneities in population densities and/or migration rates that stop such waves. We will emphasize the latter two topics, which are critical to understanding when local introductions will be successful and how far they might be expected to spread. Throughout, we will contrast the behavior of bistable systems with that of "Fisherian" systems with only one stable equilibrium. We demonstrate the utility of a one-parameter cubic approximation that focuses on the position of the unstable equilibrium. This approximation provides, for instance, empirically useful and robust sufficient conditions for initiating spatial spread from a localized introduction, as well as biological conditions, described as variation in population density, for stopping these waves. No attempt will be made to formally derive the central mathematical results, but the appendixes provide a guide to the analyses, and illustrative numerical results are provided throughout.

Models

Temporal Dynamics

We will focus on three situations that display bistable population dynamics: underdominant genetic systems, *Wolbachia* infections that produce cytoplasmic incompatibility (CI) and fitness costs, and an idealized model of Allee effects. Many other examples can be given (e.g., in game theory [Hofbauer 1999] and epidemiology [Duerr et al. 2005]), but one of our key messages is that important features of all of these systems can be understood both qualitatively and quantitatively in terms of a generic cubic model described below, which appears in the theoretical literature of population genetics, ecology, physiology, chemistry, and physics.

Underdominance. The reference system for our analyses is chromosome rearrangements, specifically translocations or inversions, that produce selection against heterozygotes, as analyzed by Barton (1979*a*). Their dynamics are well approximated by those of a diallelic locus. Other genetic models, involving epistasis among multiple loci, behave in a qualitatively similar way (Bazykin 1973; Barton 1979*a*). For one locus, let p denote the frequency of variant A_1 (which might be either an allele or a karyotype). Following Barton (1979*a*), we parameterize selection by assigning fitnesses $1 + 2S$, $1 - s + S$, and 1 to genotypes A_1A_1, A_1A_2, and A_2A_2, respectively. We set $\alpha = S/s$ to quantify the strength of directional selection versus underdominant selection and assume that $0 < \alpha < 1$ to make the heterozygotes least fit and A_1A_1 most fit. (With $-1 < \alpha < 0$, we retain underdominance, but A_2A_2 becomes the fitter homozygote.) The change per generation in p is

$$\Delta p = \frac{sp(1 - p)(2p + \alpha - 1)}{1 + 2ps(\alpha - 1 + p)}, \qquad (1)$$

so the unstable equilibrium frequency is

$$\hat{p} = \frac{1 - \alpha}{2}. \qquad (2)$$

As α approaches 1, the unstable point converges to 0, corresponding to directional selection for (recessive) A_1. With weak selection, that is, $S, s \ll 1$, as assumed by the continuous-time, continuous-space diffusion approximations of Fisher (1937), Bazykin (1969), and Barton (1979a), equation (1) is approximated by

$$\frac{dp}{dt} = sp(1 - p)(2p + \alpha - 1) = 2sp(1 - p)(p - \hat{p}). \qquad (3)$$

As shown below, approximating the dynamics by this cubic greatly facilitates analyses and provides a useful reference (and approximation) for more general models.

Cytoplasmic Incompatibility. We focus on the simplest case in which the CI-causing bacteria show perfect maternal transmission; the generalization to imperfect maternal transmission (Turelli and Hoffmann 1995) is discussed below. We assume that only a single infection type is present in the spatially distributed population. We consider both discrete-time and continuous-time models. First, we follow Caspari and Watson (1959) and assume the infection has only two effects: (i) incompatible crosses (infected male with uninfected female) produce a hatch rate of $H < 1$ relative to the hatch rate of the three other possible crosses, all of which are assumed to produce equal hatch rates, and (ii) infected females are assumed to have relative fecundity $F \le 1$ (cf. Weeks et al. 2007).

If we set $H = 1 - s_h$ and $F = 1 - s_f$ and let p denote the frequency of infected adults, the local dynamics are described by

$$\Delta p = \frac{s_h p(1 - p)(p - \hat{p})}{1 - s_f p - s_h p(1 - p)}, \qquad (4a)$$

with

$$\hat{p} = \frac{s_f}{s_h}. \qquad (4b)$$

In this model, the condition for bistability (i.e., simultaneous local stability of $p = 0$ and $p = 1$) is $s_h > s_f$; that is, the (frequency-dependent) benefit to the infection from CI must exceed the cost from decreased fecundity. With weak CI and weak fecundity effects, that is, $s_h, s_f \ll 1$, equation (4a) can be approximated by equation (3), with

$$s = \frac{s_h}{2},$$

$$\hat{p} = \frac{s_f}{s_h}. \qquad (5)$$

In contrast, the full dynamics described by equations (4) and equation (1) are not equivalent because the denominators differ slightly. The consequences of strong CI versus weak CI are discussed below.

To avoid assuming weak CI in our analysis of spatial dynamics and to accommodate possible life-shortening effects of *Wolbachia* (Min and Benzer 1997; Kambris et al. 2009; McMeniman et al. 2009) in a one-dimensional, continuous-time approximation (rather than a multidimensional age-structure model; Turelli 2010), we consider a birth-death approximation proposed by J. G. Schraiber and S. J. Schreiber (personal communication). Their model, described in appendix A, produces

$$\frac{dp}{dt} = \frac{s_h d_I p(1 - p)(p - \hat{p})}{1 - s_f p - s_h p(1 - p)}, \qquad (6a)$$

with d_I specifying the death rate for infected individuals and

$$\hat{p} = \frac{s_r}{s_h} = \frac{s_f + s_v - s_f s_v}{s_h}. \qquad (6b)$$

As in equations (4), s_h measures the intensity of CI, and s_f measures the reduction in fecundity produced by *Wolbachia* infection, whereas s_v measures decrease in mean lifetime, and s_r measures the net decrease in fitness.

Allee Effects. In general, Allee effects describe population dynamics in which the per capita growth rate is maximized at a nonzero population density, that is, population dynamics described by

$$\frac{dn}{dt} = ng(n), \qquad (7)$$

with $dg(n)/dn > 0$ for n near 0. "Strong" Allee effects (Wang and Kot 2001) describe the more extreme case in which the net population growth rate, $f(n) = ng(n)$, is negative for small n, so that the population will tend to become extinct locally unless a critical population density is reached. Rather than repeating the extensive ecological results for these models (reviewed in Lewis and Kareiva 1993; Taylor and Hastings 2005), we will simply reference them. Many of the most influential analyses are based on a quadratic approximation of $g(n)$ in equation (7) that produces the cubic model, equation (3) (e.g., Lewis and Kareiva 1993; Keitt et al. 2001).

To discuss all of these cases in a common language, we will refer to the alternative stable states as "loss" versus

"fixation." For the ecological model, "fixation" corresponds to reaching a saturation density; for the underdominance and CI models, it corresponds to $p = 1$. If weak mutation (relative to selection) is introduced into the underdominance model or if imperfect maternal transmission is introduced into a model of strong CI, the alternative stable states correspond to very low versus very high frequencies of the variants. Moving the positions of the two alternative stable states slightly has no qualitative effect on the spatial dynamics (Keener and Sneyd 2004, chap. 9.2.1).

Dynamics in Space and Time

Diffusion Approximations. Fisher (1937) and Kolmogorov et al. (1937) introduced the classical diffusion approximation for allele frequency dynamics in time and space, assuming a spatially continuous population in which frequency dynamics can be approximated by a differential equation. They presented no formal justification for this approximation. Haldane (1948, p. 279) presented a Taylor series justification, assuming that the distribution of dispersal distances is "not too leptokurtic." For discrete-time models, such as equation (1), the continuous-time analysis is usually justified by assuming weak selection, as in Slatkin (1973), Nagylaki (1975), and Barton (1979*a*). However, Turelli and Hoffmann (1991) heuristically applied Barton's (1979*a*) weak-selection partial differential equation (PDE) approximation to a natural system with strong CI by simply setting the denominator in equations (4) to 1. This ad hoc procedure is supported by numerical analyses presented below.

We assume that local dynamics can be approximated by $dp/dt = f(p)$, where time t is measured in any convenient unit such as days, years, or generations. In a one-dimensional homogeneous habitat, the spatiotemporal dynamics of variant frequencies, denoted $p(x, t)$, where x indicates position, are approximated by

$$\frac{\partial p}{\partial t} = \frac{\sigma^2}{2}\frac{\partial^2 p}{\partial x^2} + f(p). \tag{8}$$

Here σ^2 denotes the variance of distances between the birthplaces of mothers and offspring if we measure t in generations (a slightly different definition is used in two dimensions). Heuristically, this approximation assumes that the distribution of dispersal distances is not too long tailed and that local changes are not too abrupt. The robustness of the results to rapid change and highly leptokurtic dispersal can be addressed with numerical analyses or with integrodifference equations (IDEs).

Equation (8) remains largely intractable for general forms of f, but exact results are available for the cubic

approximation (eq. [3]). We will show that after time (and space) are rescaled, the cubic provides quantitatively accurate (and generally conservative) approximations for the three questions we address for more detailed models. In what sense, and to what degree, one can theoretically justify this approximation remains a challenge for further study.

Integrodifference Equations. An alternative approach to dealing with fast local dynamics (e.g., strong selection or CI) is to retain discrete time while still assuming that the population is continuously distributed in space. In this case, we start with the local dynamics

$$p(t + 1) = h(p(t)). \tag{9}$$

Assuming that local frequency dynamics are followed by dispersal and that dispersal distances are independent of location, we can approximate spatiotemporal dynamics by the IDE

$$p(x, t + 1) = \int_{-\infty}^{\infty} h(p(y, t))k(x - y)dy, \tag{10}$$

where x denotes position and $k(x)$ denotes the "dispersal kernel" (i.e., distances from the birthplaces of mothers and offspring). In general, fewer results are available for IDE models than for PDE models, but some (cited below) clarify the robustness and limitations of conclusions based on equation (8).

Wave Speed

One Dimension, Homogeneous Environment

Exact Solution for the Cubic Approximation. Equation (8) can be explicitly solved when $f(p)$ is cubic (cf. Keener and Sneyd 2004, chap. 9). It is convenient to express the solution in terms of scaled variables. Setting

$$T = st,$$

$$X^2 = \frac{2sx^2}{\sigma^2} \tag{11}$$

in equation (8) with $f(p) = 2sp(1 - p)(p - \hat{p})$, we obtain

$$\frac{\partial p}{\partial T} = \frac{\partial^2 p}{\partial X^2} + 2p(1 - p)(p - \hat{p}), \tag{12}$$

where $\hat{p} = (1 - \alpha)/2$ for underdominance, with $\alpha = S/s$ (eq. [1]) and $\hat{p} = s_r/s_h$ for CI (eqq. [6]). This same cubic model is the focus of Lewis and Kareiva's (1993) influential theoretical analysis of Allee effects for invading species (see their eq. [2]).

Assuming directional selection without dominance,

which corresponds to $f(p) = sp(1 - p)$ in equation (8), and an initial condition of the form $p(x, 0) \to 1$ as $x \to -\infty$ and $p(x, 0) \to 0$ as $x \to \infty$, Fisher (1937) sought a traveling-wave solution for equation (8), that is, a solution of the form $p(x, t) = u(x - ct)$, where c denotes the wave speed. For models like this, with a single stable equilibrium at fixation (and approximately linear dynamics near $p = 0$), there is a family of solutions with different speeds, but fluctuations at the leading edge slow the wave to the minimum speed, which is determined by $f(p)$ solely through the dynamics near $p = 0$, that is, only by the selective advantage s for directional selection (Stokes 1976). In contrast, the spatial dynamics of bistable systems depend on local dynamics averaged over all frequencies (see eq. [15]; Stokes 1976; Fife 1979b). As with Fisherian systems, the rate of spatial spread and the form of the spreading wave depend on initial conditions, but for a wide range of biologically plausible initial conditions, both the wave form and its rate of movement depend asymptotically only on the parameters of the model (Kolmogorov et al. 1937; Fife 1979a; Bramson 1983). As shown by Barton (1979a), a traveling-wave solution of equation (12) is

$$p(X, T) = \frac{1}{1 + e^{X - \alpha T}}, \qquad (13)$$

where $\alpha = 1 - 2\hat{p}$ is the scaled wave speed. Note that as $X \to \infty$, the variant frequency falls to 0, whereas as $X \to -\infty$, its frequency rises to 1. This solution assumes an initial state close to fixation to the left of an arbitrary point and absent to the right. Alternatively, the wave could spread in both directions from a local introduction, with the shape of the leading edges described by equation (13). Key features of local introductions are discussed below, but the asymptotic speed of spread is the same for all conditions that produce spread to fixation (Aronson and Weinberger 1975).

Two fundamental conclusions emerge from equation (13). First, if $\hat{p} < 1/2$ ($\alpha > 0$), the fixation state advances. For underdominant selection, this corresponds to the fitter homozygote, A_1A_1, reaching fixation everywhere. (If $-1 < \alpha < 0$, there is still underdominance, but A_2A_2 is the fitter homozygote and the fixation state [$p = 1$] retreats, so that A_1 is lost throughout the range.) For weak CI, this analysis predicts that the CI-causing infection will spread spatially only if $\hat{p} < 1/2$, corresponding to $s_h > 2s_r$. These results show a fundamental difference between isolated and spatially distributed populations. In an isolated population, any variant that shows bistable dynamics can be driven to fixation as long as enough individuals are introduced to produce an initial frequency p_0 above the unstable equilibrium $\hat{p}$. In contrast, for a population uniformly distributed in space, no local introduction, no

matter how extensive, can lead to permanent transformation throughout the species range unless the variant satisfies $\hat{p} < 1/2$. We show below that for models more general than equation (12), the condition $\hat{p} < 1/2$ for spatial spread is replaced by a constraint on the parameters (see eq. [15]) that can be interpreted as $\hat{p} < p^*$, where the value of p^* is model dependent (but always very near 1/2 for the CI models we consider).

The second conclusion is that wave speed, when measured with respect to the scaled time and space variables, is proportional to $1/2 - \hat{p}$. For the underdominance model, $\hat{p} \to 0$ corresponds to directional selection favoring a recessive allele A_1; for CI, it corresponds to an infection with no fitness cost ($s_r = 0$). As $\hat{p} \to 1/2$, corresponding to more symmetrical underdominance or increasing fecundity cost for a CI-causing microbe, the wave speed falls to 0. Thus, genetic/cytoplasmic variants with $\hat{p}$ near 1/2 will tend to spread very slowly relative to unambiguously favored variants with $\hat{p} = 0$. Ecological analyses have emphasized that Allee effects slow species invasions (e.g., Kareiva and Lewis 1993; Taylor and Hastings 2005; Tobin et al. 2007). Transforming to unscaled variables, with time measured in generations, the asymptotic velocity of spatial spread, denoted c, is

$$c = \sigma \sqrt{2s} \left(\frac{1}{2} - \hat{p} \right) \qquad (14a)$$

for the underdominance model and

$$c = \sigma \sqrt{s_h} \left(\frac{1}{2} - \hat{p} \right) \qquad (14b)$$

for the cubic approximation of CI, as given by Turelli and Hoffmann (1991).

Numerical Solution for Arbitrary f(p)*: Strong CI.* For models in which $f(p)$ is not cubic, such as the CI model (eqq. [6]), the conditions for an advancing traveling wave and the resulting wave speed can be calculated by methods used by Fisher (1937) and outlined in appendix B. A variant with continuous-time dynamics $dp/dt = f(p)$ produces a traveling wave of advance if

$$\int_0^1 f(p)\,dp > 0 \qquad (15)$$

(Stokes 1976; Fife 1979b, chap. 4). Hence, the direction of wave motion depends on dynamics averaged over all frequencies. In contrast, Fisherian variants essentially always spread, and their wave speed depends only on dynamics at the leading edge, via $f'(0)$, the rate of increase near $p = 0$ (Stokes 1976; Rothe 1981; Lewis and Kareiva

1993). For Fisherian systems, long-distance dispersal can dramatically increase wave speed (Mollison 1977; Kot et al. 1996), whereas bistable waves are much less sensitive to non-Gaussian dispersal (Wang et al. 2002). Stokes (1976) refers to these qualitatively different regimes as "pulled" versus "pushed" waves, respectively. The distinction is that a few long-distance migrants can pull a Fisherian wave forward, whereas bistable waves need sufficient migration to push the leading edge over the unstable point. (See app. B for a more detailed discussion of Stokes 1976.)

For the CI model (eqq. [6]), we can find parameter combinations that make the integral in equation (15) 0; this bounds the parameters consistent with spatial spread. These bounds can be used to specify a critical value of the unstable point, denoted p^*, such that if $\hat{p} < p^*$, the fixation state advances (i.e., $p(x, t) \to 1$ for all x as $t \to \infty$), while if $\hat{p} > p^*$, the fixation state retreats ($p(x, t) \to 0$). If $f(p) = ap(1 - p)(p - \hat{p})$, criterion (15) produces $p^* = 1/2$, as seen from the analytical solution (eq. [13]). For equations (6), we focus on complete CI ($s_h = 1$) and set $d_I = 1$ without loss of generality (this corresponds to measuring time in units of the average lifetime for infected individuals). With $s_f = 0$, $p^* = 1/2$, as in the cubic model, but as s_f increases, p^* slowly increases, reaching only 0.54 with $s_f = 0.5$. Thus, the constraints imposed by equation (15) on the parameters of the CI model (eqq. [6]) are very similar to $\hat{p} < 1/2$, which arises from the cubic approximation.

As shown by J. G. Schraiber and S. J. Schreiber (personal communication), the wave speed for the CI model (eqq. [6]) can be obtained using the method described in appendix B. It is useful to compare the numerically obtained wave speed with the cubic approximation, analogous to equation (14b),

$$c = \sigma \sqrt{\frac{s_h}{\overline{T}_I}} \left(\frac{1}{2} - \hat{p}\right) \tag{16}$$

(here time is measured in days). Figure 1 shows how the wave speed varies with $\hat{p}$ (and hence with s_v) when $s_h = 1$ and $s_f = 0$, 0.1, or 0.25, in comparison with the speed predicted by equation (16). Overall, the approximation is close to the actual wave speed but systematically underestimates it. Underestimation is expected because by ignoring the denominator in equation (6a), the cubic approximation underestimates the rate of local fixation that moves the wave forward. Because of the relative accuracy of the cubic approximation for all of the questions we address, we will focus primarily on the one-parameter spatial model (eq. [12]).

Integrodifference Result and More General Models. IDE models are valuable tools for understanding the effects of
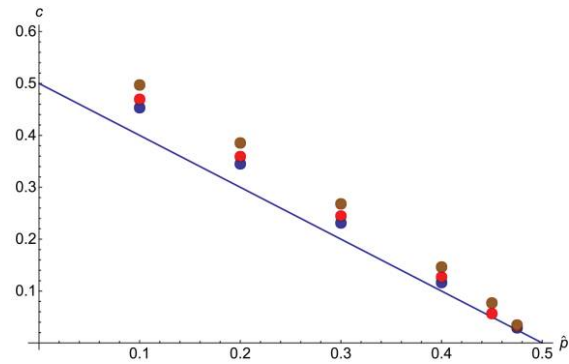
Figure 1: Comparison of the scaled wave speed calculated for the partial differential equation (eq. [8]) with $\sigma = 1$ and local dynamics described by the cytoplasmic incompatibility (CI) model (eqq. [6]) with $s_h = 1$ and $d_I = 1$ (so that $\overline{T} = 1$ in eq. [16]) to the analytical prediction (eq. [16]) based on the cubic approximation. The line is the analytical prediction for the cubic, $c = 1/2 - \hat{p}$; dots are the calculated values for the CI model with $s_f = 0$ (*blue*), 0.1 (*red*), and 0.25 (*brown*).

rapid local changes and long-tailed distributions that are incompatible with the diffusion approximation, equation (8) (Mollison 1977; Kot et al. 1996). One general result is that whether a variant spreads is independent of the form of the dispersal function, as long as it is symmetrical. Wang et al. (2002) have shown that for model (10) with symmetric dispersal, fixation spreads as a traveling wave if and only if

$$\int_0^1 (h(p) - p)dp > 0. \tag{17}$$

Because $\Delta p = h(p) - p$, this result is directly analogous to equation (15). When applied to the discrete-time CI model (eqq. [4]) with $s_h = 1$, this condition implies that the CI-inducing infection will spread only if $\hat{p} = s_f \leq 0.54$, which again is close to the constraint ($\hat{p} < 1/2$) that arises from the cubic. In contrast to wave direction, asymptotic wave speed does depend on the form of dispersal, with "heavier tails" producing faster waves. Heavy-tailed distributions, such as the Laplace (or "reflected exponential," $k(x) = (\alpha/2)e^{-\alpha|x|}$) or the more extreme exponential square root model ($k(x) - (\alpha^2/4)e^{-\alpha(|x|)^{1/2}}$), can increase wave spread well above that predicted by the reaction-diffusion PDE (eq. [12]; Schofield 2002; Wang et al. 2002). Nevertheless, as indicated by Wang et al. (2002, fig. 4) and additional numerical results kindly provided by M. Kot (personal communication), bistable (vs. Fisherian) wave speed is much less sensitive to dispersal tails, and bistable

systems do not show accelerating waves, which can occur with Fisherian systems.

Neubert and Caswell (2000) provide useful methods for calculating wave speeds in age- or stage-structured populations, but their methods are restricted to Fisherian systems (e.g., multiple loci with directional selection). No comparable results seem available for bistable systems.

Heterogeneous Environments and Two Dimensions

To understand the dynamics of spatial spread in two dimensions and the consequences of barriers to dispersal, we first consider how spatial heterogeneity affects one-dimensional waves.

Variation in Density and Dispersal in One Dimension. If population density $\rho(x)$ varies, then variants found in denser regions tend to spread because of asymmetry in net migration. To see this, consider the following generalization of equation (8) (Nagylaki 1975; Barton 1979a),

$$\frac{\partial p}{\partial t} = \frac{\sigma^2}{2}\frac{\partial^2 p}{\partial x^2} + \sigma^2\frac{\partial \log(\rho(x))}{\partial x}\frac{\partial p}{\partial x} + f(p). \quad (18)$$

If we seek a traveling-wave solution of equation (18) in the form $p(x, t) = P(x - ct)$, we find that $P(z)$ must satisfy

$$0 = \frac{\sigma^2}{2}P'' + \left[c + \sigma^2\frac{\partial \log(\rho(x))}{\partial x}\right]P' + f(P). \quad (19)$$

Thus, the form of the solution, P, will be independent of the density gradient, with the only difference being the speed. That is, if c_0 is the speed in the absence of a density gradient, the speed with a constant density gradient is

$$c = c_0 - \sigma^2\frac{\partial \log(\rho(x))}{\partial x} \quad (20)$$

(Barton 1979a). This shows that wave movement is slowed by increasing population density. A gradient in the dispersal rate, or asymmetric dispersal, induces wave movement in a way that is precisely analogous to a density gradient; hence, we assume symmetric dispersal without loss of generality (Nagylaki 1975, 1978a; Barton 1979a; Lewis and Kareiva 1993).

Equation (20) indicates that a wave traveling through a homogeneous environment at rate c_0 will be stopped if it encounters a constant population density gradient steep enough to make $c \leq 0$. This holds whether the underlying dynamics are Fisherian or bistable. In particular, a Fisherian wave can be halted or reversed if it faces an infinitely extended density gradient that is sufficiently steep. This reflects the fact that favored alleles can be swamped by sufficient immigration of less fit alleles. However, it is biologically unrealistic to consider steep density gradients of

infinite length, and unlike bistable waves, Fisherian waves will not be stopped by density gradients (or barriers to dispersal) that are bounded. The critical observation is that a small trickle of migration beyond an unfavorable density gradient would allow a Fisherian wave to continue its spread, whereas a bistable wave may be permanently halted because much more migration is necessary to push the wave into an area dominated by the alternative equilibrium. We discuss this further when we consider conditions that halt traveling waves.

Variation in dispersal can be handled similarly. With variable dispersal distances (but constant population density), the density gradient term in equation (18) is replaced by $[\partial\sigma^2(x)/\partial x](\partial p/\partial x)$; thus, a constant gradient in dispersal changes wave speed from c to $c - \partial\sigma^2(x)/\partial x$. Similarly, with asymmetric dispersal, a mean shift by a distance m per generation changes wave speed to $c - m$. These effects of variation in density and dispersal distances, and asymmetric dispersal, on wave speed hold regardless of how selection acts and apply even to multidimensional systems, described by frequencies of multiple alleles or age classes.

For the spread of a species with an Allee effect, the analogue of a density gradient might be a gradient of carrying capacity, but unlike underdominance and CI systems, the position of the unstable point is likely to change as a function of the local capacity. Asymmetric dispersal or a dispersal gradient has the same effect on species spread that it has on the spread of genetic or cytoplasmic variants (Lewis and Kareiva 1993; Lutscher et al. 2007). With a gradient in log fitness that varies in space, we expect movement at a speed proportional to the gradient averaged across the width of the wave.

Two Dimensions. Barton (1979a) and Barton and Hewitt (1989) show how the one-dimensional model and its wave-speed calculations can be extended to two dimensions. In two dimensions, we interpret σ^2 as the variance in dispersal distance along any axis. (This implies that the average Euclidean distance between the birthplaces of mothers and daughters is $\sigma(\pi/2)^{1/2}$, assuming Gaussian dispersal.) It is simplest to consider radially symmetric solutions, which provide useful guidance for the expected behavior of introductions in nature (cf. Lewis and Kareiva 1993; Soboleva et al. 2003), but this is not straightforward. With radial symmetry, the two-dimensional analogue of equation (8) is

$$\frac{\partial p}{\partial t} = \frac{\sigma^2}{2}\frac{\partial^2 p}{\partial r^2} + \frac{\sigma^2}{2r}\frac{\partial p}{\partial r} + \sigma^2\frac{\partial \log(\rho)}{\partial r}\frac{\partial p}{\partial r} + f(p). \quad (21)$$

There is no exact, radially symmetric traveling-wave solution. However, if the radius of the wavefront is large, there will be a close approximation to a one-dimensional
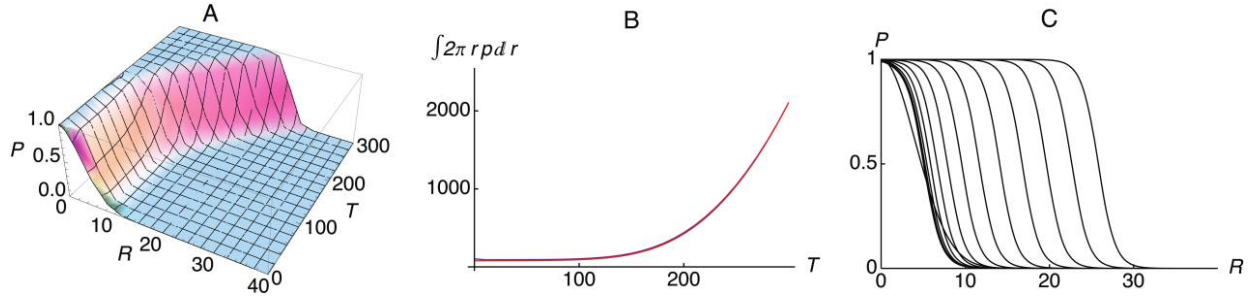
Figure 2: Comparison of wave speed in one and two dimensions for the cubic model. The dynamics are illustrated by a local introduction that is just sufficient to initiate a wave of advancing fixation. This figure illustrates a radially spreading wave starting with a Gaussian initial condition as described below. *A* shows the numerical solution of equation (21). *B* shows the area under this frequency function (*red*) and compares it with that expected if the wave were simply a cylinder of height 1 whose radius expanded according to equation (25) (*blue, under red*). *C* shows the cross section of the radially symmetric solution at (scaled) times $T = 0, 20, 40, ..., 200$. In this example, $\hat{p} = 0.35$ ($\alpha = 0.3$). The initial condition is Gaussian shaped, with the variant frequency set to 1 at the center and the variance of the Gaussian just large enough to avoid the swamping effects of migration ($V_0 = 7.81$). The constant k is chosen in equation (25) to match the numerical solution at the largest time examined (using the approximation $W(x) \sim \log(x) - \log(\log(x))$ for large x; Corless et al. 1996).

standing wave, given by the solution to equation (19) but with the coefficient of P' changed to $c + \sigma^2 \partial \log(\rho)/\partial r + \sigma^2/2r$. The radius r, of course, changes across the cline, but if the wavefront is narrow relative to the radius, then it can be taken as approximately constant. Thus, the swamping effect of gene flow changes the wave speed by $-\sigma^2/2r$, independent of $f(p)$. (More precisely, if the variant frequency gradient is negligible outside some interval $r_- < r < r_+$, then the change in wave speed must be within the range $\sigma^2/2r_+ < \Delta c < \sigma^2/2r_-$.)

The central qualitative result can be understood most simply for the scaled cubic model, described by equation (12) in one dimension. For one dimension, the wave speed in scaled units (see eq. [11]) is simply $\alpha = 2(1/2 - \hat{p})$. In two dimensions, we focus on radially symmetric waves, using the scaled units

$$R^2 = \frac{2sr^2}{\sigma^2},$$

$$T = st. \tag{22}$$

Let $Z(T)$ denote the position of the midpoint of the radially spreading wave, that is, the value of R at time T for which $p(R, T) = 0.5$. If the fixation state is spreading radially outward from an initial introduction, the scaled asymptotic wave speed is identical in one and two dimensions, but on the basis of the discussion above, the wave initially moves more slowly, with speed approximated by

$$c = \alpha - \frac{1}{Z}. \tag{23}$$

If the wave were moving at exactly the speed given by

equation (23), we could approximate the dynamics of $Z(T)$ by

$$\frac{dZ}{dT} = \alpha - \frac{1}{Z}, \tag{24}$$

which implies that

$$Z(T) = \frac{1}{\alpha}\left\{1 + W\left[e^{\alpha^2(T+k)-1}\right]\right\}, \tag{25}$$

where k is a constant that can be chosen to meet boundary conditions and $W[x]$ is defined as the real solution of $x = W[x]e^{W[x]}$ (Lambert's W function; Corless et al. 1996). For small x, $W[x] \sim x$, and for very large x, $W[x] \sim \log[x]$. Hence, as expected, the wave travels asymptotically at rate $\alpha = 2(1/2 - \hat{p})$ as long as it starts at $Z > 1/\alpha$.

The utility of these approximations is illustrated in figure 2. The numerical solution of equation (21) is closely approximated by equation (25) (fig. 2*B*). As predicted by equation (23), the wave spreads relatively slowly initially but rapidly approaches the constant asymptotic wave speed α, predicted from the one-dimensional analysis (fig. 2*C*).

Wave Initiation: Critical Propagule Size

It is obvious that a successful introduction must produce a local frequency above $\hat{p}$ because dispersal from the surrounding uninvaded area will tend to reduce p even as local dynamics are trying to increase it. However, it is not obvious how far above the unstable point the initial frequency must be or over what area the unstable equilibrium must be exceeded.

The problem of characterizing introductions that will

produce traveling waves, which we refer to as the "critical propagule size," is closely related to the problem of determining critical patch sizes (and migration rates) consistent with maintaining a locally adapted genotype or species. Critical patch size has been addressed by ecologists (Skellam 1951; Kierstead and Slobodkin 1953) and population geneticists (Slatkin 1973; Nagylaki 1975). Barton (1987) found the probability of fixation of a locally favored allele as a function of its position. For bistable dynamics, Barton (1979a) found the critical propagule size for a weakly advantageous allele, and Lewis and Kareiva (1993) dealt with the analogous ecological problem arising with Allee effects. Soboleva et al. (2003) discussed the two-dimensional problem, emphasizing the importance of the unstable equilibrium that separates the stable states.

Several questions concerning critical propagule size can be considered, including the following three, presented in descending order of difficulty. First, what is the minimum propagule size (in terms of numbers of individuals introduced) that can produce a wave of advance? This seems to be a difficult problem, with no published solution or general numerical algorithm even for the simple cubic model (eq. [12]). Second, how does the critical propagule size vary with the initial spatial profile? For instance, traveling waves assume a specific asymptotic form. Do initial propagules with this profile require fewer or more individuals than required if a constant frequency is introduced over a circle (or square or star)? This specific question is amenable to straightforward numerical analysis. A third question—likely to be directly relevant to practical applications—is even simpler to address numerically. Assuming that an introduction will produce a fixed initial frequency over a circle in two-dimensional space, how does the minimum introduction diameter needed to start a wave of advance vary with the initial frequency and the position of the unstable equilibrium? We will use the cubic approximation to show that this final question has a relatively simple and empirically useful answer and that this approximation provides a conservative bound for the CI model (eqq. [6]). However, we first illustrate some general features of introductions that lead to traveling waves in one dimension.

One Dimension: "Critical Bubbles" versus Initial Conditions Leading to Global Fixation

With dispersal, the initial frequency at the center of an introduction area must be higher than the unstable equilibrium value because migration will act to equalize frequencies across space. In general, the total number that must be introduced for fixation to spread depends on the initial configuration. In one spatial dimension, there is a unique unstable equilibrium configuration for a localized

introduction that can be explicitly calculated for the cubic approximation. When there are two stable equilibria in isolated populations, there are also two in a spatially extended population: loss everywhere or fixation everywhere. These two spatially homogeneous equilibria are separated by a family of unstable equilibria. A trivial unstable equilibrium is the spatially homogeneous one in which the frequency is everywhere at the local unstable equilibrium. More interesting solutions are symmetrical unimodal distributions that describe a "critical bubble" in which the local increase driven by the frequency dynamics $f(p)$ is exactly balanced by the local decrease caused by migration. (There is a one-dimensional family of these unstable equilibria because they can be centered anywhere, assuming spatial homogeneity; Coleman [1977] termed these "instantons.")

In one dimension, Rouhani and Barton (1987) explicitly found the critical bubble by using a method analogous to one used by Haldane (1948) in his pioneering cline article (see app. C). The frequency at the center of the bubble, denoted $\check{p}(\alpha)$, is

$$\check{p}(\alpha) = 1 - \frac{\alpha}{3} - \frac{1}{3}\sqrt{\alpha(3 + \alpha)}. \tag{26}$$

As $\hat{p} \to 0$ (i.e., $\alpha \to 1$), $\check{p}(a) \to 0$, as expected for a Fisherian system, whereas as $\hat{p} \to 1/2$ ($\alpha \to 0$), $\check{p}(a) \to 1$, indicating a local initial frequency far above the unstable equilibrium. Integrating their formula for the critical bubble, Rouhani and Barton (1987) obtained a function $M(\alpha)$ that is proportional to the total number that must be introduced to start a wave of fixation, assuming the critical bubble as the initial configuration,

$$M(\alpha) = \log\left(\frac{\sqrt{\alpha(\alpha + 3)}}{3 - \alpha - 3\sqrt{1 - \alpha}}\right). \tag{27}$$

Note that although $M(\alpha) \to \infty$ as $\alpha \to 0$ (because a very weakly favored variant with $\hat{p}$ near 1/2 cannot resist swamping very well), the total size increases only logarithmically. In general, swamping effects are stronger in two dimensions, as illustrated below. Although equation (27) provides a sufficient number to initiate global fixation, this number is not necessary. Other initial conditions that cut through the critical bubble (see eq. [C4]), for instance, a constant initial frequency p_0 over an interval of length $2L$, can initiate global fixation with a smaller initial release than predicted by equation (27). We will illustrate this in appendix C for two dimensions.

### Two Dimensions: Sufficient Conditions to Initiate an Advancing Wave

In two dimensions, there is no explicit solution analogous to equation (C4) for the critical bubble, no clear connection between the critical bubble and initial conditions sufficient to initiate a wave of advance, and no explicit solution for the form of the traveling wave (although an asymptotic approximation is available in the case of radial symmetry). In appendix C we discuss the critical bubble and key features of initial conditions that can start a wave of advance. Here, we focus on a relatively simple question of practical importance. Suppose we release in a circle of radius R, producing some maximal achievable frequency, say, $p_0 = 0.6$ or 0.8. What is the critical radius, R_{crit}, required to initiate an advancing wave of fixation, and how does R_{crit} change with p_0, $\hat{p}$, and the underlying local dynamics described by $f(p)$? We already know that for the cubic model $R_{crit} \to \infty$ as $\hat{p} \to 1/2$, but how quickly does this happen? Because numerical solutions of equation (21) with discontinuous initial conditions are difficult, we simplify further by using an initial condition with smooth edges, of the form

$$p(R, 0) = \frac{p_0}{1 + e^{n(R - R_0)}}, \tag{28}$$

where n is moderately large, for example, 10 (the value used in the calculations presented below), to reasonably approximate a step function; R is measured in scaled units (eq. [11]).

Figure 3 shows the critical radius against $\hat{p}$ for $p_0 = 0.6$ (*blue dots*) and $p_0 = 0.8$ (*red dots*). Figure 3 gives results for both the cubic model (*large dots*) and the continuous-time CI model (*small dots*; with $s_h = 1$ and $s_f = 0$ so that $\hat{p} = s_v$). Note that $R_{crit} = 0$ corresponds to a nonnegligible introduction because we use initial condition (28). An important feature of these results for the cubic is the relative insensitivity of R_{crit} to both the initial frequency and the position of the unstable point, as long as it is not too near the critical value $\hat{p} = 1/2$. In particular, an advancing wave of fixation will be produced for any $\hat{p} < 0.35$ and for any introduction frequency above about 0.6, as long as the introduction is made over a radius of about five dimensionless dispersal units. Hence, although $R_{crit} \to \infty$ as $\hat{p} \to 1/2$, relatively modest introductions can be effective as long as $\hat{p}$ is not too close to 1/2. Given the uncertainly of estimating model parameters in nature and calibrating the initial frequency produced by an experimental introduction, this provides useful guidance for field releases.

Figure 3 also shows that the values of R_{crit} obtained for the cubic model are always above those of our CI model. As in our wave-speed comparison, this result makes in-
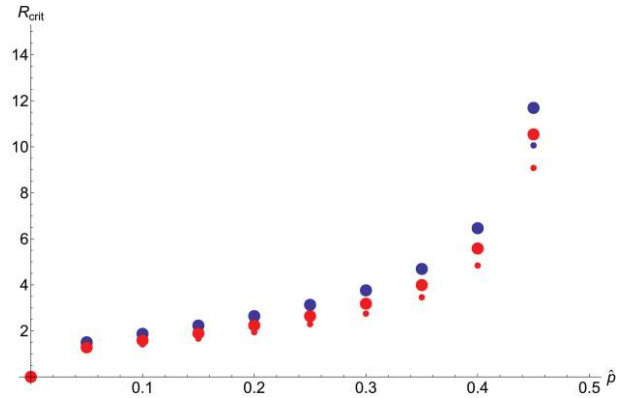
Figure 3: "Critical radii" in two dimensions as a function of the position of the unstable point $\hat{p}$. Dots are numerically determined values of the minimum radius (in units of scaled space; eq. [22]) of a release that produces an advancing wave of infection, assuming an initial frequency p_0 within a circle (see text and eq. [28] for a more precise description of the initial condition). The figure shows the effects of varying the (i) unstable point, (ii) initial frequency, and (iii) model. Blue dots correspond to $p_0 = 0.6$ and red to $p_0 = 0.8$; large dots are obtained from the cubic model and small dots from the cytoplasmic incompatibility model (eqq. [6]) with $s_h = 1$ and $s_f = 0$ (so that $\hat{p} = s_v$).

tuitive sense because the denominator in the local dynamics $f(p)$ with strong CI is less than 1, leading the cubic to underestimate the tendency of the CI-causing infection to spread. For the CI model, figure 3 focuses on the limiting case with $s_h = 1$ and $s_f = 0$ so that the single free parameter is $\hat{p} = s_v$. As expected from the heuristic argument about local dynamics, the values of R_{crit} are even smaller with $s_h = 1$ and $s_v = 0$ (so that $\hat{p} = s_f$) because the denominator of $f(p)$ is further reduced and $\int f(p)dp$ increased (see eq. [10]). For instance, with $s_h = 1$, $s_f = 0$, and $p_0 = 0.8$, R_{crit} is 1.166 (3.46) when $\hat{p} = 0.05$ (0.35) but only 1.156 (2.76) with $s_h = 1$, $s_v = 0$, and $p_0 = 0.8$. For the cubic model, the corresponding values of R_{crit} are 1.285 and 3.99. This suggests that for many models of selection-like dynamics, the cubic model may provide robust and conservative approximations for both wave speed and conditions to initiate spread. As indicated below, our simple approximations for wave initiation are also likely to be robust to changes in the exact shape of the introduction area.

To convert from the dimensionless units to physical distances, we use the scaled variables (eq. [23]). For the CI model, we can set $s = s_h d_I/2$, but the interpretation of σ^2 as the variance in dispersal distance along each axis in each generation requires $d_I = 1$. Hence, with complete CI (i.e., $s_h = 1$), the scaled spatial variable R in equation (23) and in figure 3 is simply distance measured in units of

the average standard deviation of dispersal distances per generation.

Lewis and Kareiva (1993) presented an asymptotic approximation for the critical introduction threshold when $\hat{p}$ is near 1/2. They indicate that although the asymptotic wave speed for a successful invasion is independent of the exact shape of the initial introduction, the rate of initial spread may be increased by using a "corrugated" boundary versus a "smooth" boundary for the propagule, because initial wave speed is proportional to the length of the interface between invaded and uninvaded areas (see Lewis and Kareiva 1993, pp. 154–155). The practical implication is that analyses, like those in figure 3, based on a circular introduction area likely provide a lower bound for the rate of initial spread.

Wave Stopping

As illustrated by equation (20), wave speed is affected by changes in population density and dispersal rates; a traveling wave will speed up when going "downhill" (i.e., moving from areas of higher population density and/or migration to areas with lower density/emigration). Increases in density can slow or stop both Fisherian and bistable waves. However, realistic inhomogeneities are much more likely to halt bistable "pushed" waves than Fisherian "pulled" waves because a few long-distance dispersers will not suffice to reestablish bistable wave movement. The analogous phenomenon associated with invading species subject to Allee effects is called "range pinning" (e.g., Keitt et al. 2001). Stopping bistable waves was discussed qualitatively by Bazykin (1969) and quantitatively by Barton (1979*a*) and Barton and Hewitt (1989).

In general, the movement of the tension zone between alternative stable states through a heterogeneous habitat can be understood as minimizing a potential function, defined by Barton (1979*a*) and Barton and Hewitt (1989) and described in appendix B. The tension zone moves so as to minimize its length but maximize the area covered by the "favored" state (as defined by eq. [15]). As shown by equation (20), the zone tends to move to regions of low density and dispersal. One can imagine a tension zone as a heavy elastic band that rests on a landscape whose height corresponds to the local neighborhood size (proportional to the product of local population density and variance of distances between birthplaces of mothers and offspring; Wright 1943, 1946): the zone tends to contract (minimizing the region of contact between the alternative stable states), to slide downhill, and to move outward when one type is favored over the other. As illustrated below, the effects of even mild heterogeneity in population structure (which effectively produce directionally biased dispersal) will often outweigh the inherent tendency of the interface to move (as determined by local dynamics; eq. [15]). Thus, populations are readily trapped at the "unfavorable" local equilibrium (Barton 1979*a*; Barton and Hewitt 1989). The idea of a potential function is a useful heuristic but also provides alternative derivations for some of the quantitative results described below (Barton 1979*a*).

It is easiest to understand the interaction of migration and local dynamics with discrete demes. Hence, before dealing with inhomogeneities in spatially continuous populations, we consider the much simpler case of an island that receives immigrants from a continent. This illustrates that unlike Fisherian variants, which spread for any level of migration across a metapopulation, bistable variants spread only if migration exceeds a critical threshold. Barriers in continuous space effectively reduce local migration. In appendix D, we show that as long as $\hat{p}$ is not too close to 1/2 (e.g., $\hat{p} \leq 0.35$), the simple "wave-stopping" condition derived from the mainland-island case closely approximates the conditions obtained with two populations that symmetrically exchange migrants and a linear array of discrete demes with nearest-neighbor migration. We focus on the cubic approximation (eq. [3]) but show for the simplest (island-mainland) and most complex (spatial continuum) scenarios that the CI model (eqq. [6]) produces quantitatively similar results.

Because we focus on continuous-time approximations, the interpretation of the migration parameter between discrete demes merits comment. In discrete-time models, "immigration rate" is typically the fraction of the population after immigration composed of new immigrants. If we assume a continuous immigration rate m but measure time in generations, the comparable per-generation migration parameter is $m_{\text{gen}} = 1 - e^{-m}$. For plausible migration rates, say, $m_{\text{gen}} \leq 0.2$, these parameter values are within 10% of each other.

Island-Continent Model

Following Haldane (1930), we consider an island that receives immigrants at rate m from a mainland in which a favored bistable variant (i.e., one satisfying criterion [15]) has fixed frequency p_m. Consider first the cubic model (eq. [3]), with $0 < \alpha < 1$ (and $\hat{p} = (1 - \alpha)/2$). We will contrast the cases in which the favored variant is absent ($p_m = 0$) versus fixed ($p_m = 1$) on the mainland, assuming the island is initially fixed for the opposite state. If $p_m = 0$, the equilibrium frequency on the island satisfies

$$0 = -2Mp + pq(p - q + \alpha), \qquad (29)$$

where $q = 1 - p$ and $M = m/(2s)$ is the scaled migration rate. If $M \leq M_{\text{crit}} = (1 + \alpha)^2/16 = (1 - \hat{p})^2/4$, the favored variant is maintained locally at a stable equilibrium frequency of
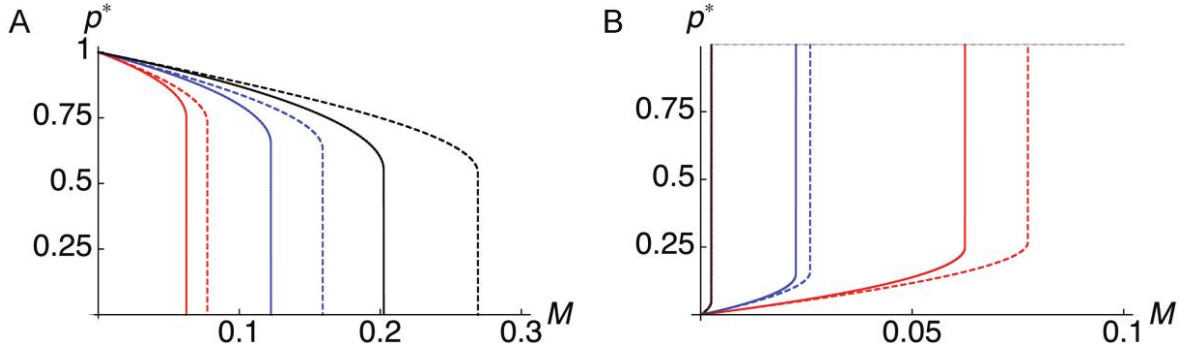
Figure 4: Equilibrium frequency in a single island, plotted against the scaled immigration rate $M = m/(2s)$ when the island is initially fixed for one stable state and the mainland is fixed for the alternative. Solid lines show the stable equilibrium p^* for the cubic model (eq. [3]) with $\hat{p} = 0.5$ (*red*), 0.3 (*blue*), and 0.1 (*black*), corresponding to $\alpha = 0$, 0.4, and 0.8, respectively. The dashed lines show the corresponding equilibria for the cytoplasmic incompatibility model (eqq. [6]) with $d_I = 1$, $s_h = 1$, and $s_f = 0$ (so that $M = m$). A, Mainland fixed for the less favored state ($p_m = 0$). B, Mainland fixed for the favored state ($p_m = 1$). Note that the scale is different in the two graphs, demonstrating how much more easily immigration of a favored equilibrium state leads to "swamping" of the island.

$$p^* = \frac{1}{4}\left|3 - \alpha + \sqrt{(1 + \alpha)^2 - 16M}\right|. \qquad (30)$$

As M increases toward $M_{\text{crit}} = (1 - \hat{p})^2/4$, the stable equilibrium frequency declines toward $(3 - \alpha)/4 = (1 + \hat{p})/2$, which is always greater than 1/2, and then collapses to 0 (fig. 4A). This qualitative observation concerning the interaction of migration and local selection originates with Haldane (1930) and was elaborated by Nagylaki (1975, 1977, chap. 6).

The equilibria for the converse case with $p_m = 1$ can be obtained by interchanging the roles of p and q in equation (29) and changing the sign of α. Hence, if $M \leq (1 - \alpha)^2/16 = \hat{p}^2/4$, the favored variant is maintained on the island at a stable equilibrium frequency of

$$p^* = 1 - \frac{1}{4}\left|3 + \alpha + \sqrt{(1 - \alpha)^2 - 16M}\right|. \qquad (31)$$

If we assume the island initially has $p = 0$ as M increases toward $M_{\text{crit}} = \hat{p}^2/4$, the stable equilibrium frequency increases gradually from 0 toward $\hat{p}/2$, which is always less than 1/4, and then it flips to 1 (fig. 4B).

It is trivial to extend these analyses to other models, and Telschow et al. (2007) have analyzed a discrete-time CI model. In figure 4, we contrast results for the cubic model (eq. [3]) with those for the CI model (eqq. [6]), assuming $d_I = 1$, $s_h = 1$, and $s_f = 0$. Note that when CI is complete, the scaled migration rate M is simply m. Figure 4A shows that the CI model behaves much like the cubic, but its denominator increases the "effective selection" by a factor $\sim 1/(1 - s_f p - s_h pq)$, which shifts the migration threshold to the right. Allowing $s_f > 0$ with $\hat{p}$ fixed shifts

the CI results slightly farther. A similar rightward shift is seen in figure 4B, suggesting that a wave of advance for CI-causing *Wolbachia* will take slightly more migration than indicated by the cubic model. A qualitatively similar but smaller effect is seen in our continuous-space analysis below.

Figure 4 shows that migration of a favored equilibrium more easily leads to "swamping" of the island, and the bias becomes increasingly pronounced as $\hat{p}$ decreases. For instance, when $\hat{p} = 0.2$, the scaled migration rate required for swamping by the favored allele is only $\hat{p}^2/4 = 0.01$, whereas the unfavored equilibrium can swamp the favored state only for $M > (1 - \hat{p})^2/4 = 0.16$. Hancock et al. (2011) use an explicit model of larval density regulation to show that the critical migration rate can vary several-fold, depending on the details of density regulation, with strong density regulation (which effectively lowers immigration) requiring higher immigration. On the other hand, their figure 1, whose parameter values produce an unstable point of $\hat{p} = 0.26$, shows that as the immigration rates increases, the stable infection frequency on the island goes from 0 to a value near 0.13 before jumping to 1, which closely matches our analytical approximation.

In appendix D, we extend this simple analysis to (i) two populations exchanging migrants at a rate m in each direction and (ii) an infinite stepping-stone of demes connected by nearest-neighbor migration at rate $m/2$ to each neighbor. For the two-population case, we seek the maximum migration rate that allows one population to remain predominately infected while the other remains predominantly uninfected. For the stepping-stone model, we seek the critical migration rate that allows all populations to the left of some point to remain predominantly infected
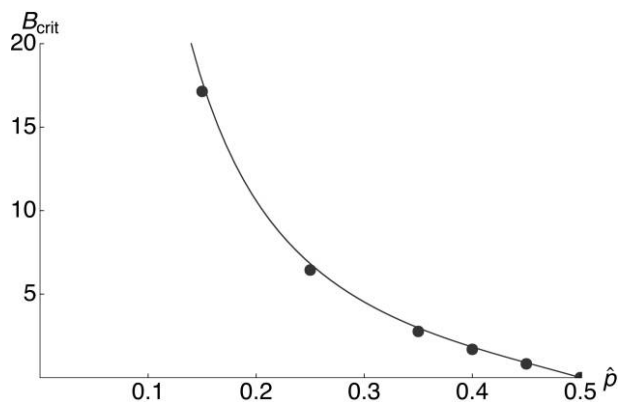
Figure 5: Curve shows the critical barrier strength, B_{crit}, just sufficient to stop wave advance, as a function of the unstable equilibrium frequency $\hat{p}$ for one dimension under the cubic model (eq. [3]). Dots show the corresponding results for the cytoplasmic incompatibility model (eqq. [6]) with $d_I = 1$, $s_h = 1$, and $s_f = 0$. See appendix D for derivation.

while those to the right remain predominantly uninfected. If $\hat{p}$ is small to moderate (e.g., $\hat{p} \leq 0.35$), the critical migration rates for both models can be very accurately approximated by the simple island-continent result with an uninfected island. Namely, with two demes, the critical scaled migration rate $M = m/(2s)$ is approximately

$$M^* = \frac{(1-\alpha)^2}{16} = \frac{\hat{p}^2}{4}. \tag{32}$$

With a linear array of demes, the migration rate to each neighbor is only half as large, so the approximate bound on M becomes

$$M^* = \frac{(1-\alpha)^2}{8} = \frac{\hat{p}^2}{2}. \tag{33}$$

Figures D1 and D2 in appendix D illustrate the accuracy of these approximations for $\hat{p} \leq 0.35$.

Continuous Populations in One and Two Dimensions

A natural framework for understanding wave stopping in continuous populations is the idea of "barrier strength," developed to describe how the flow of neutral alleles is hindered by various local obstacles. Just as a barrier to water flow in a stream will cause a sudden drop in water level, a local barrier to the diffusion of genes causes a sharp step in allele frequency, Δp, which is proportional to the allele frequency gradient on either side, $\partial p/\partial x$ (Nagylaki 1976; Barton 1979b, 1986; Barton and Bengtsson 1986). (An asymmetric barrier has different gradients to

the left and right; we discuss symmetrical local barriers first and then various sorts of asymmetrical barriers.) The strength of a localized barrier to gene flow is measured by

$$B = \frac{\Delta p}{\partial p/\partial x}, \tag{34}$$

where $\partial p/\partial x$ is the gradient adjacent to the barrier. This specifies the distance over which allele frequency would change by Δp if $\partial p/\partial x$ were to continue unchanged. To understand this measure of barrier strength, note that the net flux of neutral alleles at any point x_0 is proportional to the allele frequency gradient at that point. This can be seen as follows. The dynamics of neutral alleles diffusing in space are described by equation (8), with $f(p) = 0$. Consider a neutral allele whose frequency approaches constancy ($\partial p/\partial x = 0$) as $x \to \pm\infty$. If changes in allele frequency occur only because of migration J, the flux of alleles past x_0 must equal the net change in allele frequency to the left of x_0. Thus, using equation (8), $J = \int_{-\infty}^{x_0}(\partial p/\partial t)dx = (\sigma^2/2)\int_{-\infty}^{x_0}(\partial^2 p/\partial x^2)dx = (\sigma^2/2)(\partial p(x_0)/\partial x)$, which by definition (34) is $(\sigma^2/2)(\Delta p/B)$.

Barrier strength can be measured in several ways. Most directly, the rate at which individuals cross a point gives the flux J, which can be combined with estimates of dispersal distance to estimate $\Delta p/B$. (If the rate of individuals crossing is measured, rather than flux of a particular variant, $J = (\sigma^2/2)/B$.) If there is a cline in an effectively neutral allele or additive genetic trait, B can be estimated from $\Delta p/(\partial p/\partial x)$ (where p is interpreted as the mean trait value in the polygenic case). Finally, the scaled covariance in allele frequencies across the barrier, compared with the covariance on either side, gives an estimate of barrier strength (Nagylaki 1978b; Barton 2008). These three methods are applied by Barton and Gale (1993) to data from a chromosomal cline.

Although B is defined with reference to neutral alleles, it also usefully describes the effects of local barriers on Fisherian and bistable variants. For advantageous alleles, local barriers cause a very small delay in spread, which increases only logarithmically with B (Pialek and Barton 1997). The delay is minimal because only a few favorable alleles have to cross the barrier for spread to occur. In contrast, as illustrated by our treatment of discrete demes, much more migration is needed to permit the spread of bistable variants. Here, we determine the minimum barrier strength, denoted B_{crit}, sufficient to stop an advancing bistable variant; B has dimensions distance, and distance is scaled to $\sigma/(2s)^{1/2}$ in the usual way (see eq. [11]). After scaling, B_{crit} for the cubic model is a function only of α, or, equivalently, $\hat{p} = (1-\alpha)/2$; B_{crit} can be found numerically for any bistable variant by using the method described in appendix D. Figure 5 shows B_{crit} as a function

of $\hat{p}$ for both the cubic model (eq. [3]) and the CI model (eqq. [6]; with $s_f = 0$). Both models give very similar values, and curve fitting provides simple expressions for the limiting cases. For the cubic, B_{crit} is linear for small α ($B_{crit} \sim 9\alpha$); it diverges as $\alpha \rightarrow 1$ ($B_{crit} \sim 3.3(1 - \alpha)^{-3/2}$). Hence, as $\hat{p} \rightarrow 1/2$, a slight barrier ($B_{crit} \sim 18(1/2 - \hat{p})$) will stop the wave, whereas for low unstable thresholds, $\hat{p} \rightarrow 0$, only extreme barriers ($B_{crit} \sim 1.2\hat{p}^{-3/2}$) are effective.

Patches of Reduced Density in One Dimension. Barton (1986) shows how to calculate local barrier strength for various scenarios, the simplest being locally reduced population density or dispersal distances. Suppose that population density is constant at level ρ_0 outside of (x_1, x_2) but falls as described by $\rho(x)$ for $x_1 < x < x_2$. Starting with equation (18), which describes the effects of density variation, Barton (1986) derives

$$B = \int_{x_1}^{x_2} \left[\left(\frac{\rho_0}{\rho(x)} \right)^2 - 1 \right] dx. \tag{35}$$

Variation in dispersal, $\sigma^2(x)$, has an identical effect, and both density and dispersal variation can be treated simultaneously by replacing $\rho(x)$ in equation (35) with $\rho(x)\sigma^2(x)$, which is proportional to neighborhood size in two dimensions (Wright 1943, 1946; Barton 1986). Hence, if density (or dispersal) is reduced by roughly half over a region of length L, that would produce a barrier of strength $B_{0.5} \approx 3L$, where L is measured in the scaled spatial units used in figure 5. In contrast, a fivefold density reduction would produce $B_{0.2} \approx 24L$. For the *Wolbachia* model (eqq. [6]) with complete CI ($s_h = 1$), space is measured in units of average dispersal distances per generation over the region outside (x_1, x_2). Thus, figure 5 suggests that if $\hat{p} = 0.25$, halving population density over a patch of length 2σ would suffice to stop a *Wolbachia* wave of advance, whereas a fivefold density reduction over less than 0.3σ would stop wave motion (but see below for a more accurate analysis of small barriers). Variants with $\hat{p} = 0.15$ (0.1) would be stopped by fivefold density reduction over about 0.7σ (1.5σ), while variants with $\hat{p} = 0.4$ (0.45) would be stopped by twofold density reduction over only 0.6σ (0.3σ). Although we describe the barrier in terms of reduced population density, the wave is actually halted by the increase in density that follows, just as a ball rolling downhill can be stopped by a local dip in the surface.

This application of local barrier strength calculations is heuristic. Obviously, reducing the population density by an arbitrary amount over a distance much smaller than σ cannot affect wave behavior. Similarly, very small reductions of population density over distances that are much greater than the width of the traveling wave will also have

no effect. (If we follow Endler 1977, wave width is defined as $1/\max(|\partial p/\partial x|)$; for the cubic, this is $4\sigma/(2s)^{1/2}$.) Hence, the calculations above are expected to pertain to regions of reduced density/dispersal that are roughly between 0.5σ and $8\sigma/(2s)^{1/2}$. To quantify this intuition, we performed numerical calculations for a one-dimensional array of discrete demes linked by approximately Gaussian dispersal so that the standard deviation of the dispersal distance was roughly two demes wide (and hence most dispersal occurred within six demes). When we took a fixed number of demes, which varied from 3 to 15, density was successively lowered until the wave was just stopped. Our calculations were performed with the cubic model, assuming $s = 0.1$ and $\alpha = 0.2$, so that $\hat{p} = 0.4$. With $\sigma = 2$, the characteristic length scale $\sigma/(2s)^{1/2}$ is $20^{1/2}$. The analytical theory based on equations (34) and (35) predicts that bistable waves with $\hat{p} = 0.4$ should be stopped by local barriers (in scaled units) of $B_{crit} = 1.83$. According to equation (35), if density is reduced to a fraction ρ of the baseline over a patch of length L, $B = L(\rho^{-2} - 1)$. Hence, as L varies, one can compare the numerical values of $\rho_{crit}(\text{obs})$ with the analytically predicted values

$$\rho_{crit} = \left(1 + \frac{B_{crit}}{L} \right)^{-1/2}. \tag{36}$$

For L (measured in units of $\sigma/(2s)^{1/2}$) between 1 and 2.5, the predicted values from equation (36) are within 5% of the observed values, which range from roughly 0.6 to 0.75 (numerical results not shown). However, for longer spatial scales, the analytical theory underestimates the density reduction needed to stop the wave, as expected. For instance, with $L = 3.35$, equation (36) predicts $\rho_{crit} = 0.804$ but $\rho_{crit}(\text{obs}) = 0.754$.

Step Increases in Density in One Dimension. Real habitats can obviously involve large areas ($L \gg 1$) over which density and/or dispersal are reduced or increased. Advancing bistable waves accelerate temporarily when they encounter reduced population density and decelerate or stop when density increases (effectively because of asymmetric dispersal). To complement our analysis of symmetrical local barriers, we seek the minimum increase in population density that will stop a bistable wave. To address this, we consider wave motion across a landscape with a sharp rise in density so that the density to the right of some point, x_0, is a multiple ρ of the density to the left. Such local barriers can slow but not stop a Fisherian wave. For bistable waves, the question is, What value of ρ is just sufficient to stop wave motion? This cannot be addressed using local barrier calculations based on equation (34) but can be addressed numerically with either the diffusion approximation or discrete demes. The diffusion-based ap-

proach of appendix D can be generalized to find analytical constraints that must be satisfied by ρ_{crit}. Except for limiting cases, the resulting equations must be solved numerically. For the scaled cubic, figure 6A shows how ρ_{crit}, the critical density increase, depends on $\hat{p}$. With $\hat{p} = 0.4$, 0.25, and 0.1, $\rho_{\mathrm{crit}} = 1.31$, 2.10, and 4.53, respectively. As shown next, these results also help us understand wave stopping in two dimensions.

Invading Patches of Increased Density in Two Dimensions. In general, two-dimensional barriers have received relatively little attention, in part because they can vary infinitely in size and shape. However, our one-dimensional results concerning steps in population density suggest a natural class of two-dimensional analogues. Consider an area of radius R in which the population density increases by a factor of ρ above that of the surrounding area. If we assume the scaled cubic model, figure 6B plots the value of ρ that is just sufficient to stop wave motion as a function of R for $\hat{p} = 0.1$, 0.25, and 0.4. Note that both axes are logarithmic, so that $\hat{p} = 0.25$ produces values of ρ_{crit} much closer to those produced by $\hat{p} = 0.4$ than by $\hat{p} = 0.1$, as expected from figure 6A. Once the scaled radius R is near 10, the values of ρ_{crit} approach those found from our one-dimensional analysis of indefinitely long stretches of increased density (fig. 6A). Note that if $\hat{p} \leq 0.25$, small regions ($R \leq 1$) in which density rises even by a factor of 10 will be swamped by waves of advance of favored bistable variants.

What is most striking about these results is that even strongly "pushed" waves with $\hat{p} = 0.1$ will be unable to expand out of unfavorable habitats that support up to 20% of the population density of large adjacent regions that are more favorable. Hence, as emphasized by Barton (1979a) and Barton and Hewitt (1989), "trapped" tension zones are expected to be common in nature. Caveats are considered below.

Stochastic Effects from Finite Population Sizes and Density Fluctuations

How will random fluctuations perturb the interface between alternative equilibria? Any fluctuation in variant frequencies or in population density will ultimately shift the wave position, and the resulting drift of position can be found by averaging over the distribution of fluctuations (Barton 1979a). If the forces maintaining the interface are the same everywhere, it is possible to find general expressions for the shift caused by any initial fluctuation. These drift effects are superimposed on a base state that can be either a neutrally stable wave, say, with $\hat{p} \approx 1/2$, one whose tendency to move is just balanced by a steady density gradient or on a wave that is moving at a steady rate. Barton (1979a) showed that in one dimension, genetic drift causes the position of tension zones to move as a Brownian motion with variance $\sim w^2 t/N$, where w is the cline width and N is the number of individuals within one cline width. Random fluctuations in population density also cause a steady spatial diffusion. Density fluctuations have the greatest effect when they persist for a long time and are correlated over spatial scales of the same order as the cline width w. In two dimensions, different segments of the interface move in different directions, and so random fluctuations are much less effective: at any point, the interface will typically move $\sim t^{1/4}$ after time t, compared with $\sim t^{1/2}$ in one dimension.
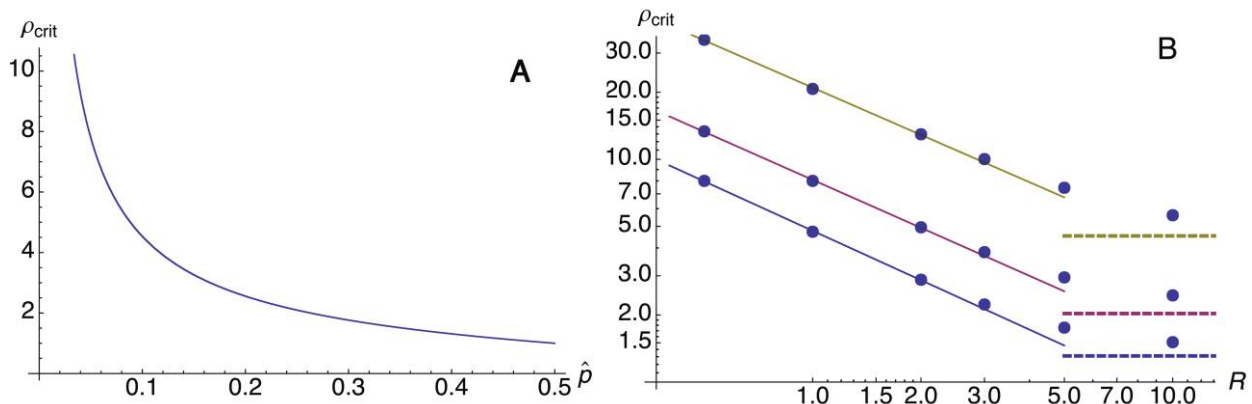
Figure 6: Increases in population density ρ that are just sufficient to stop wave advance in one (A) and two (B) dimensions under the scaled cubic model. A gives one-dimensional results for a semi-infinite step as a function of the unstable point $\hat{p}$. B presents two-dimensional results for circular regions of increased density with radius R, assuming that $\hat{p} = 0.1$ (*gold*), 0.25 (*red*), or 0.4 (*blue*). Dots are numerically determined values, slanted lines are regression fits to the numerical values, and horizontal lines are the one-dimensional results from A.

How do stochastic fluctuations alter the deterministic predictions concerning local and spatial dynamics? For isolated populations, Lande (1987) showed that demographic stochasticity can have major implications for ecological models by producing Allee-like effects. In contrast, for genetic or cytoplasmic variants, we do not expect qualitatively new effects from sampling drift, unless initial propagule sizes are extremely small, in which case the probability of local fixation can become significant in small populations even for $p_0 < \hat{p}$ (e.g., Jansen et al. 2008).

More complex stochastic effects can occur in spatially distributed populations when variation is maintained at equilibrium, preventing global fixation. We can ask at what rate will a population randomly shift from one equilibrium to a new, more favorable equilibrium? In other words, at what rate will a critical propagule be established by chance? For disruptive selection on a quantitative trait with fixed genetic variance, Rouhani and Barton (1987) analytically approximated the rate of shifts in a two-dimensional population as $\sim \exp[-Nb/(6\alpha)]$, where Nb is the neighborhood size. Thus, stochastic shifts are likely only when Nb is small and the selective asymmetry high (i.e., $\alpha \sim 1$ so that $\hat{p} \ll 1$). Also, reestablishment of the less favored state by chance is almost impossible in any large region. The most likely path during such a shift is for a small region to move to the unstable equilibrium state (eq. [B4] for small α) and then spread outward. The more biologically relevant case of underdominance at a single locus (or the simplest version of the *Wolbachia* model) is analytically intractable. However, scaling arguments and simulations show that random shifts depend in a similar way on neighborhood size and selective asymmetry (Barton and Rouhani 1991).

If the tension zone is trapped at a local barrier (e.g., a local region of low density), at what rate will it escape? Barton (1979*a*) showed that fluctuations in density are likely to be more effective than sampling drift in such a situation and gave an approximation for the rate of escape from a local density trough. If one imagines a bistable wave with $\hat{p} < 1/2$ that tends to move forward, in a heterogeneous habitat the interface can be trapped at a succession of local barriers, and its overall rate of movement will depend on the rate at which it can jump from one to the next. Barton (1979*a*, fig. 3) showed that the net rate of spatial spread can be substantially reduced by slight variations in log density.

Discussion

We have relied on two approximations to describe the spread of "bistable" variants. We approximate gene flow by spatial diffusion at a rate given by the variance of distance between parent and offspring along any axis, σ^2, and

we approximate local dynamics by a cubic function with two parameters, s and $\hat{p}$. Under these two approximations, we simplify further by expressing time and distance relative to their characteristic scales, $1/s$ and $\sigma/(2s)^{1/2}$. This leaves just one parameter to describe qualitative behavior: $\hat{p}$, the local threshold frequency above which the variant starts to increase deterministically. We have compared these approximations with more detailed models that incorporate discrete time, discrete space, and strong selection and find that they are accurate over a broad range of conditions.

Our idealized analyses do not describe the detailed dynamics of any specific system; however, we argue that they have several advantages. First, detailed models depend on many parameters, which typically cannot be measured accurately. Thus, quantitative predictions may be less informative than those from simpler, more robust approximations. Second, the role of the various parameters in a complex model is typically obscure, and so even if such models can make accurate quantitative predictions, they may still not provide much qualitative understanding. Finally, the diffusion approximation with cubic dynamics focuses attention on three key parameters (σ^2, s, and $\hat{p}$), and in many cases, it makes explicit predictions from them. Given how closely the resulting quantitative predictions match those from a more detailed model of CI, field observations should concentrate on estimating these three quantities.

Our analyses have assumed that the stable equilibria are at 0 and 1. However, mutation and imperfect maternal transmission can perturb these equilibria. For instance, in the California *Drosophila simulans–Wolbachia* system, imperfect maternal transmission and incomplete CI produced a stable equilibrium infection frequency of roughly 93% throughout the state after the wave of *Wolbachia* spread from southern California (Turelli and Hoffmann 1995; Weeks et al. 2007; Carrington et al. 2011). As shown by Keener and Sneyd (2004, chap. 9), such perturbations introduce no fundamental change in the deterministic results we discuss. The frequency variable p can simply be rescaled to (0, 1) in the same way that the dynamics of populations subject to Allee effects can be transformed by scaling population size relative to the carrying capacity. However, the effects of stochastic fluctuations do change qualitatively if the stable states are polymorphic rather than fixed; a shift to an alternative equilibrium (especially one that is favored according to criterion [15]) is greatly facilitated by initial variation (Barton and Rouhani 1991).

Implications for Population Transformation

As stated in "Introduction," our analyses were motivated by proposals to introduce cytoplasmic or genetic variants that transform insect populations to make them less harm-

ful. What are the practical implications of the results we present? First, only bistable variants that satisfy condition (15) will spread, no matter how much effort is exerted in trying to introduce them. For underdominance, this means that the unstable equilibrium for the desired variant must satisfy $\hat{p} < 1/2$, meaning that the introduced variant must be fitter as a homozygote (or homokaryotype) than the "wild type." Both the continuous-time CI model (eqq. [6]) and the corresponding discrete-time Caspari and Watson (1959) model (eqq. [4]) produce essentially the same constraint on $\hat{p}$. This result suggests that it may be difficult to control dengue fever or other diseases by releasing *Aedes aegypti* that carry the life-shortening, CI-causing *Wolbachia* wMelPop (cf. Rasgon et al. 2003; McMeniman et al. 2009). Given that wMelPop halves life length and also seems to reduce fecundity, at least under field-cage conditions (Walker et al. 2011), the analyses of Turelli (2010) and J. G. Schraiber and S. J. Schreiber (personal communication) indicate that the unstable point may be well above 1/2. However, reduced viability may not occur until late in life, and *Wolbachia* effects are likely to differ under field conditions versus laboratory conditions (Turelli and Hoffmann 1995). Moreover, life shortening may be unnecessary to control dengue with *Wolbachia* because both life-shortening (wMelPop) and non-life-shortening (wMel) *Wolbachia* from *Drosophila melanogaster* suppress various microbes, including the dengue virus, when introduced into *A. aegypti* (Moreira et al. 2009; Walker et al. 2011). Field experiments are under way to estimate the unstable point for wMel-infected *A. aegypti*. From the relatively rapid spread to near fixation of wMel in two natural Australian populations, it is plausible that $\hat{p}$ is less than 0.3, suggesting that constraint (15) will be easily satisfied (Hoffmann et al. 2011). Our numerical results indicate that the analytical wave-speed prediction (eq. [16]) provides a useful lower bound for spread in a relatively homogeneous habitat.

Perhaps our most useful result concerns the effort required to initiate spread of a bistable variant. Condition (15) sets an absolute bound on variants that can spread, but figure 3 indicates that as this bound is approached, a prohibitive effort is required to initiate the wave, which would subsequently spread only very slowly (see eqq. [14]). Hence, only variants with $\hat{p} \leq 0.35$ are plausible candidates for practical population transformation. To initiate their spread, it suffices to introduce the variant with an initial frequency above 0.6 over a circular area whose radius is on the order of five times the scaled dispersal distance, $\sigma/(2s)^{1/2}$. For *Wolbachia* variants that produce complete CI, such as wMel in *A. aegypti*, this is simply five times σ, the standard deviation of distances between the birthplaces of mothers and their offspring along any axis. As indicated by equations (14) and figure 2, the sub-

sequent wave should spread at a moderate pace. Both theoretical (Schofield 2002; Wang et al. 2002) and empirical (Turelli and Hoffmann 1991, 1995) results indicate that these predicted wave speeds may significantly underestimate actual wave speed if the dispersal distribution is highly leptokurtic, with long-distance dispersal more prevalent than expected under a Gaussian dispersal model.

Our results in figures 5 and 6 illustrate the relative ease with which bistable waves are stopped by environmental inhomogeneities that alter population densities and/or dispersal rates. These analyses indicate that even for highly favored variants, with $\hat{p}$ as low as 0.1, it is much easier to initiate a wave of advance than to insure its continued spread. Relatively minor increases in population density produce asymmetrical dispersal that can trap a traveling wave. In general, bistable waves will move at a constant rate across a homogeneous landscape and accelerate when they encounter negative gradients of population density. However, unlike Fisherian variants that can effectively jump over local increases in population density, bistable waves are relatively easily stopped by such barriers. The existence of hybrid zones, which in northern latitudes typically formed by secondary contact after the last glaciation (Barton and Hewitt 1985), indicates that such interfaces may be trapped by local barriers or environmental transitions for thousands of generations. This point is emphasized by figure 6, which indicates the levels of population density variation that are likely to halt waves of favored variants. An important caveat is that our analyses assume that the spreading variants do not significantly alter population sizes. There is currently no evidence for appreciable population-size effects associated with *Wolbachia* spread, but Hancock et al. (2011) have shown that such effects can alter quantitative predictions about introduction rates needed to initiate spread.

Our wave-stopping predictions have important practical implications. Attempts at population transformation involving localized introduction should begin in areas of relatively high population densities that will serve as sources for spread into surrounding areas with equal or lower density. Waves emanating from such sources will spread until they reach areas where they are forced to move up density gradients or jump barriers to dispersal. Hence, to transform large spatial areas, one can either initiate the wave at many local density peaks or choose one and then seed other population peaks with individuals collected from the surrounding lower-density areas once the variant has spread. Notably, after an introduced wave has begun to propagate successfully, no additional releases of lab-reared individuals may be needed.

Ecological Implications

For populations subject to Allee effects, the unstable equilibrium $\hat{p}$ can be interpreted as the fraction of the carrying capacity at which the per capita growth rate becomes positive. Several ecological reviews (e.g., Taylor and Hastings 2005; Tobin et al. 2007) have focused on the role of Allee effects in slowing range expansions. As shown by equations (23) and (24) and illustrated in figure 2 (cf. eq. [16] of Lewis and Kareiva 1993), such waves initially spread very slowly and then accelerate to the asymptotic speed described by equations (14). This initial acceleration of invasion fronts subject to Allee effects was emphasized in Viet and Lewis's (1996) analysis of house sparrow spread. As noted by Lewis and Kareiva (1993), asymptotic speed is proportional to $(1/2 - \hat{p})$.

Given our focus on purposeful introductions, our results concerning wave initiation in figure 3 can perhaps be best interpreted ecologically as guidelines for introducing (or reintroducing) species subject to Allee effects. However, our deterministic analyses provide simple rules of thumb that can be confounded by stochastic effects and environmental heterogeneity (e.g., Leung et al. 2004; Schreiber and Lloyd-Smith 2009). Our discussion of wave stopping with discrete demes is analogous to the "range-pinning" results of Keitt et al. (2001). Our approximation (33) concerning the minimum amount of (scaled) migration that produces an advancing (vs. trapped) wave describes the numerical results illustrated in their figure 3. This is expected, given that their discrete-deme population dynamic model (Keitt et al. 2001, eq. [4]) is equivalent to our stepping-stone model for variant frequencies (eq. [D6]).

The ecological interpretation of our results concerning spatial heterogeneity for continuously distributed populations is more subtle because Allee effects are expected to be proportional to absolute population sizes. Hence, as carrying capacities change spatially, we would expect $\hat{p}$ to change as well. Specifically, as carrying capacities fall, we expect values of $\hat{p}$ produced by Allee effects to rise, so that species invasions are likely to be stopped by falling carrying capacity. In contrast, for bistable genetic and cytoplasmic variants, we expect the unstable point to remain relatively constant across environmental gradients and the resulting waves would tend to be stopped by local increases, rather than decreases, in population density.

Implications for Wolbachia Population Biology and General Evolutionary Processes

Wolbachia came to the attention of population biologists through Laven's (1951, 1959) description of a patchwork of bidirectionally incompatible variants of *Culex pipiens* across Europe and northern Africa. Laven (1959) suggested that maternally inherited incompatibility might contribute to speciation, an idea that has been championed by Werren and his collaborators (e.g., Werren 1998). Hoffmann and Turelli (1997) conjectured that the contact zones between the alternative *Culex* types could be interpreted as trapped tension zones. This conjecture can be tested by determining the geographic stability of the mosaic of incompatible types or by assessing whether their boundaries occur at barriers to dispersal. Such tests remain to be done. Models of stable *Wolbachia* tension zones have been reviewed by Engelstädter and Telschow (2009), and these models have been adapted to examine whether such tension zones might lead to speciation by reinforcement (Telschow et al. 2005, 2007). Both theoretical and empirical analyses indicate that relatively narrow contact zones are not conducive to reinforcement (Sanderson 1989; Noor 1999; Turelli et al. 2001; Servedio and Noor 2007). Consistent with this expectation, the only empirical example of *Wolbachia*-associated reinforcement involves a pair of *Drosophila* species showing unidirectional incompatibility and broadly overlapping ranges (Jaenike et al. 2006).

The most perplexing feature of our analyses is that relatively slight density variation should stop bistable *Wolbachia* waves, yet there is at least one empirical example of rapid spread across hundreds of kilometers of heterogeneous rural landscape (Turelli and Hoffmann 1995). This example is confounded by extensive human-mediated dispersal (Turelli and Hoffmann 1991). It may also be confounded by the fact that *Wolbachia*-conferred protection from natural viruses (Hedges et al. 2008; Teixeira et al. 2008) may eliminate the unstable equilibrium in some times or places, making the wave Fisherian rather than bistable (cf. Jaenike et al. 2010; Himler et al. 2011). Recently initiated field releases of *Wolbachia*-infected *A. aegypti* (Hoffmann et al. 2011) will provide data for testing of our wave-stopping and wave-speed predictions. Spreading waves can ratchet forward through seasonal and/or random environmental fluctuations that push the unstable equilibrium or local densities downward, even when average conditions suggest that waves should be trapped (Barton 1979*a*).

It has been argued that the movement of tension zones plays a role in both adaptation and speciation—most notably in Sewall Wright's (1931) "shifting balance" theory of adaptation and M. J. D. White's (1968) model of "stasipatric speciation." Incipient species are distinguished by genetic incompatibilities that will necessarily be maintained at a sharp interface when the diverging populations meet in a parapatric distribution. For speciation to be completed, further differences must accumulate at the tension zone until reproductive isolation is complete and/or ecological divergence allows sympatry. Random movement

of the tension zone may usually cause loss of one or another form before this process can lead to speciation. The prevalence of hybrid zones makes it likely that they play some role in speciation, though this may be simply as a marker of essentially allopatric divergence.

The movement of tension zones is central to Wright's (1931) "shifting balance" theory of adaptation. Wright supposed that species are typically subdivided into a myriad of regions, each close to a different "adaptive peak." Better-adapted peaks tend to spread for a variety of reasons, all involving movement of the tension zones that separate them. While Wright's theory has been influential in motivating studies of population structure, little attention has been paid to the directional movement required for it to be a systematically adaptive process (though see Mallet and Joron 1999). Coyne et al. (1997) review the many reasons that make selection among "adaptive peaks," as envisaged by Wright (1931), an implausible general contributor to adaptation, compared with selection among individuals. Though the theory we have reviewed and extended was originally developed to understand how movement of tension zones may contribute to adaptation and speciation, its applications to biocontrol and species invasions are likely to be more important.

APPENDIX A

Continuous-Time Cytoplasmic Incompatibility Model

J. G. Schraiber and S. J. Schreiber (personal communication) have proposed a continuous-time, deterministic birth-death model of cytoplasmic incompatibility (CI) that allows for viability effects without requiring the multidimensional age-structured formalism proposed by Turelli (2010). Their model has five parameters: $H = 1 - s_h$, describing CI intensity as in equations (4), plus two describing the birth rates for infected versus uninfected (b_I and b_U) and two describing their death rates (d_I and d_U). We can quantify fecundity effects with $b_I/b_U = 1 - s_f$ and viability effects with $d_U/d_I = 1 - s_v = \overline{T_I}/\overline{T_U}$, where $\overline{T_I} = 1/d_I$ is the mean life span of infected individuals. The infection frequency dynamics can be approximated by

$$\frac{dp}{dt} = \frac{p(1-p)[b_I d_U - b_U(pH + 1 - p)d_I]}{pb_I + (1-p)b_U[pH + (1-p)]}. \quad (A1)$$

This produces the equilibrium infection frequency

$$\hat{p} = \frac{1 - (b_I d_U/b_U d_I)}{s_h} = \frac{s_f + s_v - s_f s_v}{s_h}, \quad (A2)$$

which is identical to the equilibrium expression derived by Turelli (2010, see eq. [17]) for a discrete-time model of overlapping generations, assuming a stable age distribution and that the intrinsic growth rate of a monomorphic infected population is 1. As noted by J. G. Schraiber and S. J. Schreiber (personal communication), b/d corresponds to the net reproductive rate in this continuous-time model. Thus, if we set $b_I/d_I = r_I$ and $b_U/d_U = r_U$ and define $r_U/r_I = 1 - s_r$, the unstable equilibrium becomes

$$\hat{p} = \frac{s_r}{s_h}, \quad (A3)$$

which generalizes equation (4b). Similarly, equation (A1) can be rewritten as equation (6a), which provides a continuous-time analogue of equations (4) that accounts for both viability and fecundity effects. With weak CI and small fecundity effects, that is, $s_h, s_f \ll 1$, equation (6a) reduces to equation (3), with

$$s = \frac{s_h d_I}{2},$$

$$\alpha = 1 - 2\left(\frac{s_r}{s_h}\right). \quad (A4)$$

APPENDIX B

Wave Speed

Direct Calculation of Wave Speed

We first review the classical method for determining wave speed, as discussed, for instance, by Keener and Sneyd (2004, chap. 9). In one dimension with spatially homogeneous density and (symmetric) dispersal, we focus on monotone-decreasing traveling-wave solutions $p(x, t) = P(x - ct) = P(z)$, for which $P(z) \to 1$ as $z \to -\infty$, $P(z) \to 0$ as $z \to \infty$, and $dP(z)/dz \to 0$ as $z \to \pm\infty$. From equation (8), $P(z)$ must satisfy

$$0 = \frac{\sigma^2}{2} \frac{d^2 P}{dz^2} + c \frac{dP}{dz} + f(P). \tag{B1}$$

If we multiply equation (B1) by dP/dz and then integrate over all z, the first term on the right vanishes because $dP/dz \to 0$ as $z \to \pm\infty$, the second term is $c\int (dP/dz)^2 dz$, and the final term is $\int_{-\infty}^{\infty} f(P)(dP/dz)dz$, which is just $-\int_0^1 f(P)dP$. Hence, c satisfies

$$c = \frac{\int_0^1 f(P)dP}{\int_{-\infty}^{\infty}(dP/dz)^2 dz}, \tag{B2}$$

which implies that the sign of $\int_0^1 f(P)dP$ determines the sign of c (i.e., criterion [15]). In particular, $p(x, t)$ increases for ever-increasing x as t increases if $\int_0^1 f(P)dP > 0$.

To find c, we follow Fisher (1937) and think of dP/dz, the slope of the monotonic traveling-wave solution, as a function of P rather than z, so that $d^2P/dz^2 = (d/dz)dP/dz = (d/dP)(dP/dz)dP/dz$. If we let $G(P) = dP/dz$, equation (B1) becomes a first-order, nonlinear ordinary differential equation for the gradient $G(P)$,

$$0 = \frac{\sigma^2}{2} G \frac{dG}{dP} + cG + f(P), \tag{B3}$$

with boundary conditions $G(0) = G(1) = 0$. As argued by Keener and Sneyd (2004, chap. 9), for bistable systems, there is a unique c that produces a solution for equation (B3) satisfying these boundary conditions. Near 0, we expect the solution to be approximately linear, so that $G(P) = \lambda P$ with $\lambda > 0$ (because increasing P corresponds to decreasing z). Equation (B3) produces a quadratic for λ whose relevant solution is

$$\lambda = \frac{1}{2\sigma^2}\left(-c + \sqrt{c^2 - 2\sigma^2 f'(0)}\right). \tag{B4}$$

If we start with a trial value of c and a small initial value $P_0 \ll 1$, equation (B4) produces an initial value problem for equation (B3) that can be easily solved numerically to obtain $G(1)$. The goal is to find a value of c for which the numerical solution satisfies $G(1) = 0$. This procedure, the standard "shooting method" for solving nonlinear boundary value problems (Faires and Burden 2002, chap. 11), reduces the search for c to finding the root of a nonlinear equation defined in terms of numerical solutions to equation (B3).

If $f(P) > 0$ for $0 < P < 1$, corresponding to $P = 1$ being the only stable equilibrium, equation (B3) leads to a family of traveling-wave solutions: narrow clines that move slowly or broad clines that move rapidly. For $f'(0) > 0$, there is a unique minimum wave speed, $c_{\min} = (2\sigma^2 f'(0))^{1/2}$. If $f(P) < Pf'(0)$ for $0 < P < 1$, the traveling wave converges to this speed (Fisher 1937; Kolmogorov et al. 1937; Stokes 1976). In this case (termed a "pulled wave" by Stokes

[1976]), the speed is determined by the rate of increase at the leading edge. In contrast, if $f(P) < Pf'(0)$ for some P, there is a minimum wave speed larger than $(2\sigma^2 f'(0))^{1/2}$ that is determined by the full form of $f(P)$. Stokes (1976) termed this a "pushed wave." This term covers the bistable models we analyze and some cases of uniformly favorable alleles, for example, a favorable recessive, for which $f'(0) = 0$.

A Potential Function

Consider the general version of the scaled one-dimensional model (eq. [12]),

$$\frac{\partial p}{\partial T} = \frac{\partial^2 p}{\partial X^2} + f(p). \tag{B5}$$

Let $F(p) = \int^p f(y)dy$. We focus on spatial spread; hence, we consider a spatial position Y where the spreading variant has already reached fixation and define

$$H = \int_Y^{\infty} \left[\frac{1}{2}\left(\frac{\partial p}{\partial X}\right)^2 - F(p)\right]dX. \tag{B6}$$

Thus,

$$\frac{\partial H}{\partial T} = \int_Y^{\infty} \left(\frac{\partial p}{\partial X}\frac{\partial^2 p}{\partial X \partial T} - \frac{\partial F(p)}{\partial p}\frac{\partial p}{\partial T}\right)dX. \tag{B7}$$

Using integration by parts to evaluate the first term, assuming $\partial p/\partial X \to 0$ as $X \to \pm\infty$, we find

$$\frac{\partial H}{\partial T} = -\int_Y^{\infty} \frac{\partial p}{\partial T}\left(\frac{\partial^2 p}{\partial X^2} + f(p)\right)dX = -\int_{-\infty}^{Y}\left(\frac{\partial p}{\partial T}\right)^2 dX, \tag{B8}$$

as noted by Barton (1979*a*). Hence, the dynamics described by equation (B5) minimize H at equilibria. The first term in equation (B6) represents the effects of dispersal, which reduces the squared gradient, and the second term represents the effects of the local dynamics, $f(p) = \partial F/\partial p$. Note that when applied to one-locus selection, $F(p)$ is not mean fitness, which may decrease under the joint effects of selection and migration.

The potential function can be used to heuristically calculate how the basic wave solution (eq. [13]) is affected by various perturbations without explicitly solving the associated partial differential equations. We assume that p decreases monotonically from 1 to 0. Consider a wave of constant shape traveling at constant speed, which is currently centered at some point Z. For the cubic model,

$$H = \int_Y^\infty \frac{1}{2}\left[\left(\frac{\partial p}{\partial X}\right)^2 - p^2\left[q^2 - \alpha\left(1 - \frac{2p}{3}\right)\right]\right]dX. \quad \text{(B9)}$$

As the wave moves, there is a constant contribution to H that is independent of the position of the wave from the first term in equation (B9) and from the second term across the transitional region over which p decreases from 1 to 0. An additional contribution of the second term changes linearly with the wave position Z. If we denote the wave speed by c, $dZ/dT = c$. In the region where $p = 0$, the second term on the right-hand side of equation (B9) contributes 0; in the region where $p = 1$, it contributes $-\alpha/3$. Hence, as Z moves, $H = $ constant $-\alpha Z/6$ so that $\partial H/\partial T = -\alpha c/6$. To determine wave speed, note that for a traveling wave equation (B8) implies

$$\frac{\partial H}{\partial T} = -c^2\int_Y^\infty \left(\frac{\partial P}{\partial Z}\right)^2 dZ = -c^2\int_0^1 \frac{\partial P}{\partial Z}dP. \quad \text{(B10)}$$

Using the wave solution (eq. [13]), $\partial P/\partial Z = P(1 - P)$, so this final integral is just 1/6. Hence, $c = \alpha$. In this case, we already know the wave speed, but the argument above can be used even when we do not, if we can assume that the wave shape is approximated by equation (13), so that $\partial H/\partial T = -c^2/6$. Extensions of the potential to two dimensions are presented and applied by Barton (1979*a*) and Barton and Hewitt (1989).

APPENDIX C

Critical Propagule Size

Critical Bubble in One Dimension

We consider the "critical bubble" in one dimension, that is, the unimodal unstable equilibrium. The central results are presented by Rouhani and Barton (1987), who draw on the method outlined by Coleman (1977). They show that the critical bubble for the scaled equation (12) with $f(p) = pq(p - q + \alpha)$ (and $q = 1 - p$) must satisfy

$$\left(\frac{\partial p}{\partial X}\right)^2 = 2\int^p f(y)dy = p^2\left[q^2 - \alpha\left(1 - \frac{2p}{3}\right)\right]. \quad \text{(C1)}$$

(This follows from eq. [B1] with $c = 0$; also see eq. [D9].) The frequency at the center of the bubble, denoted $\check{p}(\alpha)$, satisfies $\partial p/\partial X = 0$, so from equation (C1),

$$\check{p}(\alpha) = 1 - \frac{\alpha}{3} - \frac{1}{3}\sqrt{\alpha(3 + \alpha)}. \quad \text{(C2)}$$

Rouhani and Barton (1987) used equation (C1) to find

the bubble shape under which the effects of local dynamics and dispersal just balance at each X. If we consider that $X > 0$ as a function of p and assume that the bubble is centered at $X = 0$, equation (C1) implies that

$$\frac{\partial X}{\partial p} = \frac{1}{p\sqrt{\{q^2 - \alpha[1 - (2/3)p]\}}}. \quad \text{(C3)}$$

If we integrate equation (C3) and assume that the bubble is centered at 0, the value of $X > 0$ that produces each value of $p < \check{p}(\alpha)$ is

$$X = \frac{1}{\sqrt{1 - \alpha}}\log\left\{\frac{3}{p\sqrt{\alpha(3 + \alpha)}}\left[1 - p - \alpha\left(1 - \frac{p}{3}\right)\right.\right.$$
$$\left.\left. + \sqrt{1 - \alpha}\sqrt{(1 - p)^2 - \alpha\left(1 - \frac{2p}{3}\right)}\right]\right\}. \quad \text{(C4)}$$

An important feature of this curve is that any initial spatial configuration $p(x, 0)$ that is everywhere above equation (C4) will produce a traveling wave leading to global fixation. Conversely, any initial configuration $p(x, 0)$ that is everywhere below equation (C4) will produce global loss. By integrating equation (C4) over space, we obtain a function $M(\alpha)$ (eq. [27]) that is proportional to the total number that must be introduced to start a wave of fixation, assuming that the configuration is equation (C4).

Critical Bubble versus Critical Propagule Size in Two Dimensions

We can seek a critical initial propagule size that will be just sufficient to allow spread and that minimizes the numbers released. Any initial condition that is just sufficient to allow spread defines a critical surface that separates the alternative outcomes of loss or fixation: we term these "critical initial distributions." On the basis of extensive numerical analyses, we find that trajectories near these critical initial distributions evolve toward a characteristic "critical bubble," an unstable equilibrium in two dimensions analogous to equation (C4), before expanding to fixation or collapsing to loss. We can trace the total numbers as the population evolves along this path: the solution we seek must minimize the initial number but produce increasing numbers (e.g., fig. C1*B*). Soboleva et al. (2003) show that asymmetric initial states (e.g., an asymmetric [correlated] Gaussian, concentrated along one axis; their fig. 4) can spread, even if its maximum height is lower than that of the critical bubble. Our numerical calculations of the same model confirm this. However, our calculations show that any critical initial distribution that just allows spread evolves toward the symmetrical critical bubble and

that critical initial distributions that minimize either mass or maximum height are symmetrical. One can also find asymmetric critical initial distributions, which may have lower mass or height than the critical bubble, but as far as we can tell, these do not minimize the mass or the maximum frequency required. The subtle connection between critical initial distributions and the critical bubble is easiest to understand in a limiting case.

Although the critical bubble has not been analytically determined for two dimensions, it can be approximated as $\hat{p} \to 1/2$ ($\alpha \to 0$), corresponding to the limit at which invasion is slowest. As shown by Rouhani and Barton (1987), for small α, the bubble is large, with scaled radius, denoted R^*, proportional to $1/\alpha$ and cross section proportional to $1/[1 + e^{(R-R^*)}]$. This is roughly a radially symmetric version of the traveling-wave solution (eq. [13]) in one dimension. It suggests that in two dimensions, when $\hat{p}$ is near 1/2 (α small), the introduced type must be spread over a very large area to overcome swamping. Note that as $\alpha \to 0$, critical bubble size (analogous to $M(\alpha)$ in eq. [27]) increases as $1/\alpha$ in two dimensions but only as $-\log(\alpha)$ in one dimension. (Lewis and Kareiva [1993]

also show that the critical radius for successful introduction approaches infinity at the rate $(1/2 - \hat{p})^{-1}$.) This indicates that the swamping effects of dispersal are significantly greater in two dimensions, as indicated in our discussion of wave speed (see eq. [23]). In addition, this asymptotic solution illustrates that the minimum number needed to initiate a wave of advance may be much smaller than the number under the critical bubble. To see this, consider a population with small α. The critical bubble has the invading type close to fixation within a circle of radius ~$1/\alpha$. Yet an introduction of approximately half as many individuals, with frequency just over $\hat{p} = 1/2$ within the circle, will increase to near fixation within the circle, approach the critical bubble, and then spread outward, as illustrated in figure C1. Figure C1 illustrates that when we begin near a critical initial distribution, the local frequency dynamics leading to near fixation in the introduction area occur on a much more rapid timescale than spatial spread. Because initial introductions substantially smaller than suggested by the critical bubble can initiate waves of fixation, characterizing the critical bubbles is not central to engineering successful introductions.
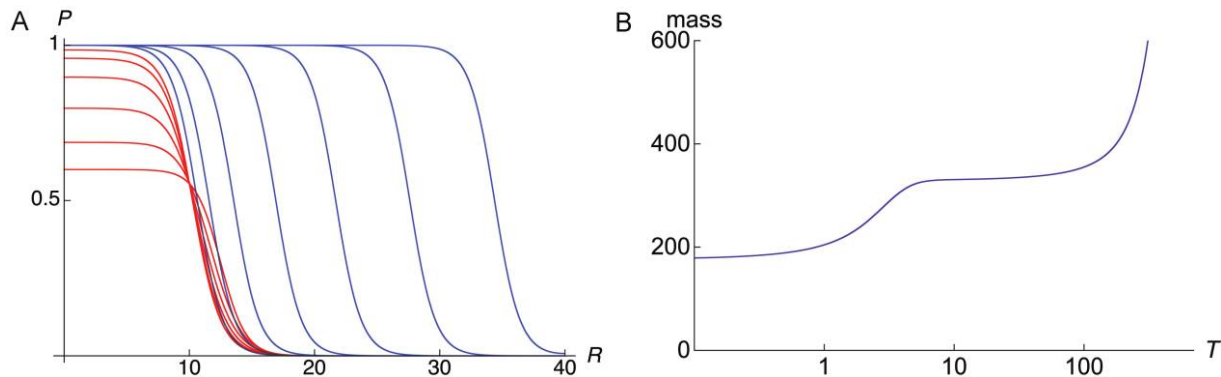
Figure C1: Wave initiation and speed in two dimensions, illustrated by a local introduction that is just sufficient to initiate a wave of advancing fixation. The calculations use the scaled cubic model with $\alpha = 0.1$ ($\hat{p} = 0.45$), and *B* illustrates the distinctive timescales of local frequency increase versus spatial spread. With $\alpha \ll 1$, spread requires the radius of the initial introduction to be rather larger than $1/\alpha$ and the frequency larger than $\hat{p} = (1 - \alpha)/2 = 0.45$. We used $p_0 = 0.6$ and $R_0 = 12.5$, which is just above the critical propagule size. *A* shows the rapid initial local increase at $T = 0, 1, \ldots, 5$ (*red*), which is followed by the much slower subsequent spread ($T = 100, 200, \ldots, 700$; *blue*). Throughout, the fit to $c = \alpha - (1/R)$ (not shown) is extremely close. *B* shows the increase of total mass (area under the frequency distribution) over time; note the logarithmic scale. The mass rapidly increases locally at the critical bubble but then hovers there before continuing to global fixation.

APPENDIX D

Stopping Waves

The island-mainland model can be analyzed with simple algebra. We will outline the derivations and heuristic arguments relevant to our results for two demes, the stepping-stone model, and diffusion approximations for barriers in continuous space.

Two Demes

Consider two demes with symmetric migration at rate m. We seek the maximum migration rate that can produce a stable equilibrium at which one deme is near $p = 0$ and the other near $p = 1$. Flor et al. (2007) considered this question for cytoplasmic incompatibility (CI), and Engelstädter and Telschow (2009) review several related CI models. If we denote the frequencies of the favored variant in the two demes p_1 and p_2, the equilibria satisfy

$$0 = 2M(p_2 - p_1) + p_1 q_1(p_1 - q_1 + \alpha), \tag{D1a}$$

$$0 = 2M(p_1 - p_2) + p_2 q_2(p_2 - q_2 + \alpha), \tag{D1b}$$

where, as in equation (29), $q_i = 1 - p_i$ and $M = m/(2s)$ is the scaled migration rate. For sufficiently low migration, the favored type can always be stably maintained at low frequency in one deme and high frequency in the other (Karlin and MacGregor 1972).

To obtain the critical value of M, we simultaneously solve the equations for the equilibrium allele frequencies (eqq. [D1]) and set to 0 the determinant of the matrix that determines stability of these equilibria (corresponding to passing from stability to instability when 0 becomes an eigenvalue of the stability matrix). If we let $f(p) = pq(p - q + \alpha)$, with $q = 1 - p$, and use the abbreviations $f_i = f(p_i)$, $f'_i = f'(p_i)$, and $\Delta = p_1 - p_2$, the equations to be solved are

$$2M\Delta = f_2 = -f_1, \tag{D2a}$$

$$2M(f'_1 + f'_2) = f'_1 f'_2. \tag{D2b}$$

If we set $\omega = p_1 + p_2 - 1$, these equations are satisfied when

$$\omega = -\frac{\alpha}{3} + \frac{\phi}{6},$$

$$\Delta = \frac{1}{6} \sqrt{4(3 + \alpha^2) + 5\phi^2},$$

$$p_1 = \frac{1 - \Delta + \omega}{2}, \tag{D3}$$

$$p_2 = \frac{1 + \Delta + \omega}{2},$$

where $\phi = \alpha^{1/3}(9 - \alpha^2)^{1/3}$. From equation (D2a),

$$M_{\text{crit}} = \frac{f_2}{2\Delta} = \frac{1}{36}[3 + \alpha^2 - \alpha^{2/3}(9 - \alpha^2)^{2/3}], \tag{D4}$$

which is $\sim(1 - \alpha)/16$ for $\alpha \sim 1$ (i.e., $M_{\text{crit}} \sim \hat{p}^2/4$ for $\hat{p} \sim 0$) and $\sim[(1/12) - (\alpha/3)^{2/3}/4]$ for $\alpha \sim 0$.

As shown in figure D1, for $\hat{p} \le 0.4$, M_{crit} is only slightly higher than

$$M^* = \frac{(1 - \alpha)^2}{16} = \frac{\hat{p}^2}{4}, \tag{D5}$$

which is the value of M_{crit} obtained from the island-mainland analysis when the island initially lacks the favored variant. If $\hat{p} \le 0.2$, $M > 0.01$ leads to fixation of the favored variant in both demes, whereas if $\hat{p} = 0.3$ and $M \le 0.02$, the unfavored variant is maintained. In contrast, in the Fisherian case ($\hat{p} = 0$), both demes always fix the favored variant for any $m > 0$.

Stepping-Stone of Discrete Demes with Nearest-Neighbor Migration

We again assume the cubic model (eq. [3]) and consider an infinite array of demes, each of which exchanges migrants at rate $m/2$ with its two neighbors. Thus, although the total immigration rate is m for each deme, the rate of exchange

for adjacent demes is only half that of the two-deme model. The analogue of the scaled one-dimensional partial differential equation (eq. [12]) is a set of coupled ordinary differential equations:

$$\frac{dp_i}{dT} = M(p_{i+1} - 2p_i + p_{i-1}) + p_iq_i(p_i - q_i + \alpha), \tag{D6}$$

where p_i denotes the frequency of the favored variant in deme i, $q_i = 1 - p_i$, $T = st$, and $M = 2s/m$ is the scaled migration rate.

This model was analyzed by Barton (1979a) in the limit when α was near 0, so that $\hat{p}$ is near 1/2. Barton (1979a) estimated the critical α needed to overcome the pinning effect as a function of scaled deme spacing, defined by $\varepsilon = 1/M^{1/2}$, which was assumed to be small; that is, he sought a lower bound on α consistent with wave movement for a fixed small value of ϵ. Rewriting Barton's (1979a) lower bound on α as an upper bound on $\hat{p}$, denoted $\hat{p}^*$, yields

$$\hat{p}^* = \frac{1}{2} - 64\pi^5M^2 \exp\left(-2\pi^2\sqrt{M}\right). \tag{D7}$$

Note that for each fixed $\hat{p}$, the curve (D7) approximates M_{crit}, the lower bound on M consistent with wave movement.

For smaller values of M, a much simpler approximation is available. When the migration rate is insufficient for wave propagation, the natural "stalled wave" can be described by having $p_i = 1$ in all the demes to the left of some point but $p_i = 0$ for all demes to the right. For migration just sufficient to start wave motion, the interaction of the two adjacent demes with $p_i = 1$ and $p_{i+1} = 0$ dominates (Lande 1985). This is the two-deme case just considered. If we take into account that the migration rate between adjacent demes is $m/2$ in this model instead of m, as in the two-deme case, this heuristic approximation for M_{crit} is simply

$$M^* = \frac{(1 - \alpha)^2}{8} = \frac{\hat{p}^2}{2}. \tag{D8}$$

Figure D2 compares the analytical approximations (D7) and (D8) with numerically determined values of M_{crit}. As in the two-deme case, approximation (D8) slightly underestimates the true critical migration rate, but it is extremely accurate for $\hat{p} \le 0.35$. In contrast, approximation (D7) is very accurate for $M \ge 0.4$, corresponding to $\hat{p} > 0.495$. Given that wave movement is expected to be extremely slow in this case, we focus on the simpler approximation (D8). The accuracy of this approximation indicates that our simple island and two-deme calculations provide useful insight into the conditions for wave movement in one-dimensional stepping-stone models. What is surprising is that "nearest-neighbor" effects dominate up to $\hat{p} = 0.35$. For general mathematical results on spatially discrete models, see Chow and Mallet-Paret (1995).

Wave-Stopping Local Barriers in Continuous Space

We will present a derivation of the critical barrier strength. We illustrate the case of cubic $f(p)$, for which key integrals can be explicitly calculated, but the method applies to arbitrary $f(p)$. To understand the consequences of local barriers, one must relate the discontinuity in variant frequencies across a barrier to the gradients on either side. We consider equation (B5), the general version of the scaled equation (12). If the wave is trapped by a barrier at X_0, $\partial p/\partial T = 0$. Proceeding as in appendix B (and Haldane 1948), we multiply equation (B5) by $\partial p/\partial X$ and integrate to infinity on either side of the barrier. We assume that the variant frequency is p_0 to the left of the barrier and p_1 to the right and that $p(X) \to 0$ as $X \to -\infty$, $p(X) \to 1$ as $X \to \infty$, and $\partial p/\partial X \to 0$ as $X \to \pm\infty$.

Integrating to the left of X_0,

$$\int_{-\infty}^{X_0} \frac{1}{2}\frac{\partial}{\partial X}\left(\frac{\partial p}{\partial X}\right)^2 dX + \int_{-\infty}^{X_0} f(p)\frac{\partial p}{\partial X} dX = 0. \tag{D9}$$

The first term is half the square of the gradient $\partial p/\partial X$, approaching X_0 from the left. We denote this gradient $G_L^2(p_0)$. The second term is $\int_0^{p_0} f(p)dp$. For the scaled cubic, $f(p) = p(1 - p)(2p - 1 + \alpha)$ so that

$$G_L(p_o) = p_0 \sqrt{q_0^2 - \alpha\left(1 - \frac{2p_0}{3}\right)}, \tag{D10}$$

where $q_0 = 1 - p_0$. Similarly, the analogue of equation (D9), integrating to the right, produces an expression for the gradient to the right of the barrier, $G_R^2(p_1) = 2\int_{p_1}^{1} f(p)dp$. For the scaled cubic,

$$G_R(p_1) = q_1 \sqrt{p_1^2 - \frac{\alpha}{3}(1 + 2p_1)}. \tag{D11}$$

Note that in general

$$G_R^2(p) - G_L^2(p) = 2\int_0^1 f(p)dp; \tag{D12}$$

for the cubic, this is $\alpha/3$. The function $G_L^2(p) = \int^p f(y)dy$ also appears in the potential H described in appendix B. If we assume symmetric dispersal, the gradients on either side of the barrier must be equal; let $G = G_L(p_o) = G_R(p_1)$. Given definition (34) of barrier strength B, the value of B that is just sufficient to stop the wave must be the minimum value that satisfies

$$B = \frac{\Delta p}{G} = \frac{p_1 - p_0}{G}. \tag{D13}$$

The key to applying this condition is interpreting equation (D13) as a function of G. This function can be understood by plotting $G_R^2(p)$ and $G_L^2(p)$ against p. Given equation (D12), these functions have identical shapes, with $G_R^2(p)$ displaced above $G_L^2(p)$ by a positive constant. This implies that $G_L(p_o) = G_R(p_1) = G$ uniquely specifies a value of $\Delta p = p_1 - p_0$ (we assume $p_1 > p_0$) for each value of G^2 between 0 and the maximum of $G_L^2(p)$ over $0 < p < 1$. We seek the value of G that minimizes equation (D13). It must be found numerically even if $G_L(p_o)$ and $G_R(p_1)$ can be expressed analytically as in equation (D12). The numerical solutions are shown in figure 5 for the cubic and CI models.

In the main text, we present numerically determined approximations for the barrier strength when α is near 0 or 1. For $\alpha \ll 1$, the unstable equilibrium is near 1/2, and the wave is only weakly "pushed." Hence, we expect that a small barrier will stop it and that $p_0 \approx p_1 \approx 1/2$. In this case, $B_{crit} \approx 9\alpha = 18(1/2 - \hat{p})$. Conversely, when $\alpha \ll 1$, the unstable point is near 0. In this case, an extreme barrier is needed to stop wave movement, and we expect $p_0 \approx 0$ and $p_1 \approx 1$. For the cubic case, we numerically found $B_{crit} \approx 3.3(1 - \alpha)^{-3/2} \approx 1.2\hat{p}^{-3/2}$.
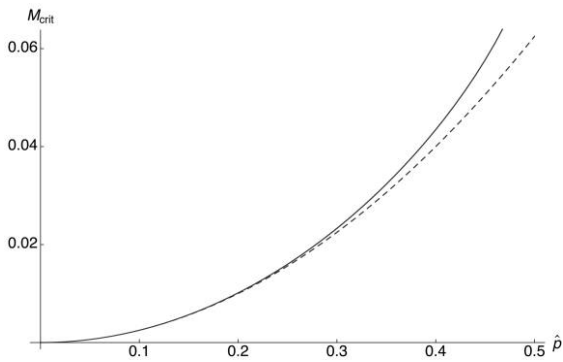
Figure D1: Solid line shows the critical value, M_{crit}, of the scaled migration rate ($M = m/(2s)$) below which a favored equilibrium can be trapped in one of two demes, plotted against the unstable equilibrium $\hat{p}$ for the cubic model (eq. [3]). Note that for $\hat{p} \le 0.35$, M_{crit} is only very slightly higher than $M^* = \hat{p}^2/4$ (*dashed line*).
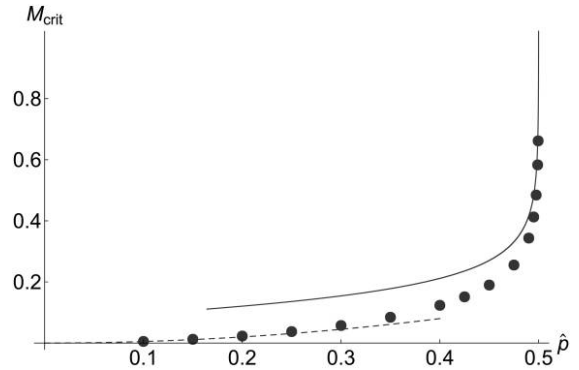
Figure D2: Dots show the numerically determined critical values, M_{crit}, of the scaled migration rate ($M = m/(2s) = 1/\varepsilon^2$) needed to allow movement along a linear stepping-stone of demes, plotted against the unstable equilibrium frequency $\hat{p}$ for the cubic model (eq. [3]). Dotted curve is the approximation $M^* = \hat{p}^2/2$ obtained from our two-deme analysis (eq. [D8]), which is accurate for $\hat{p} \le$

0.35; solid curve shows approximation (D7) from Barton (1979*a*), which is accurate for $\hat{p} \sim 0.5$.

Literature Cited

Aronson, D. G., and H. F. Weinberger. 1975. Nonlinear diffusion in population genetics, combustion, and nerve impulse propagation. Pages 5–49 *in* J. A. Goldstein, ed. Partial differential equations and related topics. Lecture Notes in Mathematics 446. Springer, New York.

Barton, N. H. 1979*a*. The dynamics of hybrid zones. Heredity 43: 341–359.

———. 1979*b*. Gene flow past a cline. Heredity 43:333–339.

———. 1986. The effects of linkage and density-dependent regulation on gene flow. Heredity 57:415–426.

———. 1987. The probability of establishment of an advantageous mutation in a subdivided population. Genetical Research 50:35–40.

———. 2008. The effect of a barrier to gene flow on patterns of geographic variation. Genetics Research 90:139–149.

Barton, N. H., and B. O. Bengtsson. 1986. The barrier to genetic exchange between hybridizing populations. Heredity 56:357–376.

Barton, N. H., and K. S. Gale. 1993. Genetic analysis of hybrid zones. Pages 13–45 *in* R. G. Harrison, ed. Hybrid zones and the evolutionary process. Oxford University Press, Oxford.

Barton, N. H., and G. M. Hewitt. 1985. Analysis of hybrid zones. Annual Review of Ecology and Systematics 16:113–148.

———. 1989. Adaptation, speciation and hybrid zones. Nature 341: 497–503.

Barton, N. H., and S. Rouhani. 1991. The probability of fixation of a new karyotype in a continuous population. Evolution 4:499–517.

Bazykin, A. D. 1969. Hypothetical mechanism of speciation. Evolution 23:685–687.

———. 1973. Population genetic analysis of disrupting and stabilising selection. 2. Adjacent populations and populations with continuous area. Genetika 9:156–166.

Bramson, M. 1983. Convergence of solutions of the Kolmogorov equation to traveling waves. Memoirs of the American Mathematical Society 44:1–190.

Brownstein, J. S., E. Hett, and S. L. O'Neill. 2003. The potential of virulent *Wolbachia* to modulate disease transmission by insects. Journal of Invertebrate Pathology 84:24–29.

Carrington, L. B., J. R. Lipkowitz, A. A. Hoffmann, and M. Turelli. 2011. A re-examination of *Wolbachia*-induced cytoplasmic incompatibility in California *Drosophila simulans*. PLoS ONE 6:e22565.

Caspari, E., and G. S. Watson. 1959. On the evolutionary importance of cytoplasmic sterility in mosquitoes. Evolution 13:568–570.

Chow, S. N., and J. Mallet-Paret. 1995. Pattern formation and spatial chaos in lattice dynamical systems. IEEE Transactions on Circuits and Systems I: Fundamental Theory and Applications 42:746–751.

Coleman, S. 1977. Fate of the false vacuum: semiclassical theory. Physical Review D 15:2929–2936.

Corless, R. M., G. H. Gonnet, D. E. G. Hare, D. J. Jeffrey, and D. E. Knuth. 1996. On the Lambert *W* function. Advances in Computational Mathematics 5:329–359.

Coyne, J. A., N. H. Barton, and M. Turelli. 1997. A critique of Wright's shifting balance theory of evolution. Evolution 51:643–671.

Curtis, C. F. 1968. Possible use of translocations to fix desirable genes in insect pest populations. Nature 218:368–369.

Duerr, H.-P., K. Kietz, and M. Eichner. 2005. Determinants of the eradicability of filarial infections: a conceptual approach. Trends in Parasitology 21:88–96.

Endler, J. A. 1977. Genetic variation, speciation, and clines. Princeton University Press, Princeton, NJ.

Engelstädter, J., and A. Telschow. 2009. Cytoplasmic incompatibility and host population structure. Heredity 103:196–207.

Faires, J. D., and R. L. Burden. 2002. Numerical methods. 3rd ed. Brooks/Cole, Belmont, CA.

Fife, P. C. 1979*a*. Long time behavior of systems of bistable nonlinear diffusion equations. Archive for Rational Mechanics and Analysis 70:31–46.

———. 1979*b*. Mathematical aspects of reacting and diffusing systems. Springer, Berlin.

Fife, P. C., and J. B. McLeod. 1977. Approach of solutions of nonlinear diffusion equations to traveling front solutions. Archive for Rational Mechanics and Analysis 65:335–361.

Fisher, R. A. 1937. The wave of advance of advantageous genes. Annals of Eugenics 7:355–369.

Flor, M., P. Hammerstein, and A. Telschow. 2007. *Wolbachia*-induced unidirectional cytoplasmic incompatibility and the stability of infection polymorphism in parapatric host populations. Journal of Evolutionary Biology 20:696–706.

Haldane, J. B. S. 1930. A mathematical theory of natural and artificial selection. VI. Isolation. Proceedings of the Cambridge Philosophical Society 26:220–230.

———. 1948. The theory of a cline. Journal of Genetics 48:277–284.

Hancock, P. A., S. P. Sinkins, and H. C. J. Godfray. 2011. Population dynamic models of the spread of *Wolbachia*. American Naturalist 177:323–333.

Hedges, L. M., J. C. Brownlie, S. L. O'Neill, and K. N. Johnson. 2008. *Wolbachia* and virus protection in insects. Science 322:702.

Himler, A. G., T. Adachi-Hagimori, J. E. Bergen, A. Kozuch, S. E. Kelly, B. E. Tabashnik, E. Chiel, et al. 2011. Rapid spread of a bacterial symbiont in an invasive whitefly is driven by fitness benefits and female bias. Science 332:254–256.

Hodgkin, A. L., and A. F. Huxley. 1952. A quantitative description of membrane current and its application to conduction and excitation in nerve. Journal of Physiology 117:500–544.

Hofbauer, J. 1999. The spatially dominant equilibrium of a game. Annals of Operations Research 89:233–251.

Hoffmann, A. A., and M. Turelli. 1997. Cytoplasmic incompatibility in insects. Pages 42–80 *in* S. L. O'Neill, J. H. Werren, and A. A. Hoffmann, eds. Influential passengers: inherited microorganisms and arthropod reproduction. Oxford University Press, Oxford.

Hoffmann, A. A., B. L. Montgomery, J. Popovici, I. Iturbe-Ormaetxe, P. H. Johnson, F. Muzzi, M. Greenfield, et al. 2011. Successful establishment of *Wolbachia* in *Aedes* populations to suppress dengue transmission. Nature, doi:10.1038/nature10356.

Jaenike, J., K. A. Dyer, C. Cornish, and M. S. Minhas. 2006. Asymmetrical reinforcement and *Wolbachia* infection in *Drosophila*. PLoS Biology 4:e325.

Jaenike, J., R. Unckless, S. N. Cockburn, L. M. Boelio, and S. J. Perlman. 2010. Adaptation via symbiosis: recent spread of a *Drosophila* defensive symbiont. Science 329:212–215.

Jansen, V. A. A., M. Turelli, and H. C. J. Godfray. 2008. Stochastic spread of *Wolbachia*. Proceedings of the Royal Society B: Biological Sciences 275:2769–2776.

Kambris, Z., P. E. Cook, H. K. Phuc, and S. P. Sinkins. 2009. Immune

activation by life-shortening *Wolbachia* and reduced filarial competence in mosquitoes. Science 326:134–136.

Karlin, S., and J. MacGregor. 1972. Application of method of small parameters to multi-niche population genetic models. Theoretical Population Biology 3:186–209.

Keener, J., and J. Sneyd. 2004. Mathematical physiology. Springer, New York.

Keitt, T. H., M. A. Lewis, and R. D. Holt. 2001. Allee dynamics and the spread of invading organisms. American Naturalist 157:203–316.

Key, K. H. L. 1968. The concept of stasipatric speciation. Systematic Zoology 17:14–22.

Kierstead, H., and L. B. Slobodkin. 1953. The size of water masses containing plankton blooms. Journal of Marine Research 12:141–147.

Kolmogorov, A. N., I. Petrovsky, and N. Piscounoff. 1937. Etude de l'equation de la diffusion avec croissance de la quantile de matiere et son application a un probleme biologique. Bulletin of the State University of Moscow A: Mathematics and Mechanics 1:1–25.

Kot, M., M. A. Lewis, and P. van den Driessche. 1996. Dispersal data and the spread of invading organisms. Ecology 77:2027–2042.

Lande, R. 1985. The fixation of chromosomal rearrangements in a subdivided population with local extinction and recolonisation. Heredity 54:323–332.

———. 1987. Extinction thresholds in demographic models of territorial populations. American Naturalist 130:624–635.

Laven, H. 1951. Crossing experiments with *Culex* strains. Evolution 5:370–375.

———. 1959. Speciation by cytoplasmic isolation in the *Culex pipiens* complex. Cold Spring Harbor Symposia on Quantitative Biology 24:166–173.

Leung, B., J. M. Drake, and D. M. Lodge. 2004. Predicting invasions: propagule pressure and the gravity of Allee effects. Ecology 85:1651–1660.

Lewis, M. A., and P. Kareiva. 1993. Allee dynamics and the spread of invading organisms. Theoretical Population Biology 43:141–158.

Lutscher, F., E. McCauley, and M. Lewis. 2007. Spatial patterns and coexistence mechanisms in systems with unidirectional flow. Theoretical Population Biology 71:267–277.

Magori, K., and F. Gould. 2006. Genetically engineered underdominance for manipulations of pest populations: a deterministic model. Genetics 172:2613–2620.

Mallet, J. L. B., and M. Joron. 1999. Evolution of diversity in warning color and mimicry: polymorphisms, shifting balance, and speciation. Annual Review of Ecology and Systematics 30:201–233.

McMeniman, C. J., R. V. Lane, B. N. Cass, A. W. C. Fong, M. Sidhu, Y. Wang, and S. L. O'Neill. 2009. Stable introduction of a life-shortening *Wolbachia* infection into the mosquito *Aedes aegypti*. Science 323:141–144.

Min, K. T., and S. Benzer. 1997. *Wolbachia*, normally a symbiont of *Drosophila*, can be virulent, causing degeneration and early death. Proceedings of the National Academy of Sciences of the USA 94:10792–10796.

Mollison, D. 1977. Spatial contact models for ecological and epidemic spread. Journal of the Royal Statistical Society B 39:283–326.

Moreira, L. A., I. Iturbe-Ormaetxe, J. A. Jeffery, G. Lu, A. T. Pyke, L. M. Hedges, B. C. Rocha, et al. 2009. A *Wolbachia* symbiont in *Aedes aegypti* limits infection with dengue, chikungunya, and *Plasmodium*. Cell 139:1268–1278.

Nagumo, J., S. Arimoto, and S. Yoshizawa. 1962. An active pulse transmission line simulating nerve axon. Proceedings of the Institute of Radio Engineers 150:2061–2070.

Nagumo, J., S. Yoshizawa, and S. Arimoto. 1965. Bistable transmission lines. IEEE Transactions on Circuit Theory 12:400–412.

Nagylaki, T. 1975. Conditions for the existence of clines. Genetics 80:595–615.

———. 1976. Clines with variable migration. Genetics 83:867–886.

———. 1977. Selection in one- and two-locus systems. Springer, Berlin.

———. 1978a. Clines with asymmetric migration. Genetics 88:813–827.

———. 1978b. A diffusion model for geographically structured populations. Journal of Mathematical Biology 6:375–382.

Neubert, M. G., and H. Caswell. 2000. Demography and dispersal: calculations and sensitivity analysis of invasion speed for structured populations. Ecology 81:1613–1628.

Nichols, R. A., and G. M. Hewitt. 1986. Population structure and the shape of a chromosomal cline between two races of *Podisma pedestris* (Orthoptera: Acrididae). Biological Journal of the Linnean Society 29:301–316.

Noor, M. A. F. 1999. Reinforcement and other consequences of sympatry. Heredity 83:503–508.

Pialek, J., and N. H. Barton. 1997. The spread of an advantageous allele across a barrier: the effects of random drift and selection against heterozygotes. Genetics 145:493–504.

Rasgon, J. L., L. M. Styer, and T. W. Scott. 2003. *Wolbachia*-induced mortality as a mechanism to modulate pathogen transmission by vector arthropods. Journal of Medical Entomology 40:125–132.

Rothe, F. 1981. Convergence to pushed fronts. Rocky Mountain Journal of Mathematics 11:617–633.

Rouhani, S., and N. Barton. 1987. Speciation and the "shifting balance" in a continuous population. Theoretical Population Biology 31:465–492.

Sanderson, N. 1989. Can gene flow prevent reinforcement? Evolution 43:1123–1235.

Schofield, P. 2002. Spatially explicit models of Turelli–Hoffmann *Wolbachia* invasive wave fronts. Journal of Theoretical Biology 215:121–131.

Schreiber, S. J., and J. O. Lloyd-Smith. 2009. Invasion dynamics in spatially heterogeneous environments. American Naturalist 174:490–505.

Servedio, M. R., and M. A. F. Noor. 2007. The role of reinforcement in speciation: theory and data. Annual Review of Ecology, Evolution, and Systematics 34:339–364.

Shigesada, N., and K. Kawasaki. 1997. Biological invasions: theory and practice. Oxford University Press, Oxford.

Sinkins, S. P., and F. Gould. 2006. Gene drive systems for insect disease vectors. Nature Reviews Genetics 7:427–435.

Skellam, J. G. 1951. Random dispersal in theoretical populations. Biometrika 38:196–218.

Slatkin, M. 1973. Gene flow and selection in a cline. Genetics 75:733–756.

Soboleva, T. K., P. R. Shorten, A. B. Pleasants, and A. L. Rae. 2003. Qualitative theory of the spread of a new gene into a resident population. Ecological Modelling 163:33–44.

Stokes, A. N. 1976. On two types of moving front in quasilinear diffusion. Mathematical Biosciences 31:307–315.

Taylor, C. M., and A. Hastings. 2005. Allee effects in biological invasions. Ecology Letters 8:895–908.

Teixeira, L., A. Ferreira, and M. Ashburner. 2008. The bacterial symbiont *Wolbachia* induces resistance to RNA viral infections in *Drosophila melanogaster*. PLoS Biology 6:e2.

Telschow, A., P. Hammerstein, and J. H. Werren. 2005. The effect of *Wolbachia* versus genetic incompatibilities on reinforcement and speciation. Evolution 59:1607–1619.

Telschow, A., M. Flor, Y. Kobayashi, P. Hammerstein, and J. H. Werren. 2007. *Wolbachia*-induced unidirectional cytoplasmic incompatibility and speciation: mainland-island model. PLoS ONE 8: e701.

Tobin, P. C., S. L. Whitmire, D. M. Johnson, O. N. Bjornstad, and M. Liebhold. 2007. Invasion speed is affected by geographical variation in the strength of Allee effects. Ecology Letters 10:36–43.

Turelli, M. 2010. Cytoplasmic incompatibility in populations with overlapping generations. Evolution 64:232–241.

Turelli, M., and A. A. Hoffmann. 1991. Rapid spread of an inherited incompatibility factor in California *Drosophila*. Nature 353:440–442.

———. 1995. Cytoplasmic incompatibility in *Drosophila simulans*: dynamics and parameter estimates from natural populations. Genetics 140:1319–1338.

Turelli, M., N. H. Barton, and J. A. Coyne. 2001. Theory and speciation. Trends in Ecology & Evolution 16:330–343.

Viet, R. R., and M. A. Lewis. 1996. Dispersal, population growth, and the Allee effect: dynamics of the house finch invasion of eastern North America. American Naturalist 148:255–274.

Walker, T., P. H. Johnson, L. A. Moreira, I. Iturbe-Ormaetxe, F. D. Frentiu, C. J. McMeniman, Y. S. Leong, et al. 2011. The *w*Mel *Wolbachia* strain blocks dengue and invades caged *Aedes aegypti* populations. Nature, doi:10.1038/nature10355.

Wang, M.-H., and M. Kot. 2001. Speeds of invasion in a model with strong or weak Allee effects. Mathematical Biosciences 171:83–97.

Wang, M.-H., M. Kot, and M. G. Neubert. 2002. Integrodifference equations, Allee effects, and invasions. Journal of Mathematical Biology 44:150–168.

Weeks, A. R., M. Turelli, W. R. Harcombe, K. T. Reynolds, and A. A. Hoffmann. 2007. From parasite to mutalist: rapid evolution of *Wolbachia* in natural populations of *Drosophila*. PLoS Biology 5:e114.

Werren, J. H. 1998. *Wolbachia* and speciation. Pages 245–260 *in* D. J. Howard and S. H. Berlocher, eds. Endless forms: species and speciation. Oxford University Press, New York.

White, M. J. D. 1968. Models of speciation. Science 158:1065–1070.

———. 1973. Animal cytology and evolution. Cambridge University Press, Cambridge.

Whitten, M. J. 1971. Insect control by genetic manipulation of natural populations. Science 171:682–684.

Wright, S. 1931. Evolution in Mendelian populations. Genetics 16: 97–159.

———. 1943. Isolation by distance. Genetics 28:307–320.

———. 1946. Isolation by distance under diverse systems of mating. Genetics 31:39–59.

Zeldovich, Y. B., and G. I. Barenblatt. 1959. Theory of flame propagation. Combustion and Flame 3:61–74.